Dear Editor,

We are very thankful for the reviewers' comments. In response to these we have extensively revised the manuscript. We now explain in more detail how we combine LEFM and viscous flow, the process of crevasse initiation, the hypotheses we made and the limitations of our approach. We fixed minor typos, added Figure 7 and Figure 8, modified a number of figures to improve clarity, modified our description of the undercutting experiment, improve the comparison of modeled crevasses versus observed crevasses. These modifications improved the manuscript significantly but do not affect our conclusions. We hope you will find the paper acceptable for publication.

1 Response to Reviewer Till Wagner

Detailed below are our point-by-point responses to the comments of Reviewer Till Wagner. Reviewer's comments are printed in blue font followed by our responses in black.

The authors develop a 2D ice-sheet model that includes the time-evolution of crevasses, by combining a Full Stokes (FS) model with an account of linear elastic fracture mechanics (LEFM). The results are compared to those obtained with higher-order (HO) and shallow-shelf approximations (SSA). The model is set up to represent a cross-section of Thwaites Glacier (TG), and the model output is compared to observed crevasses at TG. The results suggest that deviations from hydrostatic equilibrium are an important driver of crevasse propagation, and ultimately calving.

The study is concerned with a pressing topic in glaciology and climate science, and offers an innovative approach to the calving problem. A physically consistent combination of the FS model and LEFM under consideration of both surface and basal crevasses would constitute significant progress. The paper is furthermore clearly presented, well written, and nicely illustrated. There are a few major points that I believe should be addressed. These are (i) a discussion of issues involving the complex rheology of ice, particularly that of combining a viscous flow model with an elastic fracture model (ii) the question of crevasse initiation; (iii) a more direct comparison with the observational crevasse data, and (iv) a more detailed analysis of the stress conditions that lead to crevasse propagation in LEFM. I will discuss these, together with a number of more minor comments, below.

Overall, I believe that this manuscript will - after some revisions - be a valuable contribution to the literature and a significant step toward adequately representing glacier calving in ice sheet and climate models.

Major Comments

1. The manuscript offers little discussion of the potential issues and limitations of its approach, and fails to put methods and results sufficiently into context with the existing literature. For one, LEFM is fundamentally somewhat at odds with the non-linear viscous-plastic rheology of glacier ice (e.g., Weiss (2004); Benn et al. (2007), a topic that merits at least some discussion. A particular issue is that of the different timescales of the viscous flow model and the LEFM crevasse propagation. In the paper, the LEFM routine is called every 20th time step of the FS model routine. Some justification or motivation for this particular coupling scheme should be given.

Yes, the LEFM and viscous theories act on different time scales: the LEFM is essentially instantaneous (or the speed of sound) while the viscous flow takes place on the time scale of days to months. It is also correct that the LEFM cannot explain some aspects of crevasse propagation. Weiss (2004) argued that LEFM cannot explain the initiation of crevasse from mm to m scale and proposed a subcritical crack propagation method. Here, we do not need this method because our focus is the propagation of crevasses, not their initiation. However, this means that our LEFM model requires a minimum crevasse depth. Here, we assume that the crevasses propagate from infinitesimal crevasses that are always present in glacier ice and we assume they can propagate if their required depth is less than 1 m. According to LEFM, the width of crevasse should be in the order of $\sim$1 cm. It is computational too demanding to have mesh resolution at this scale. We therefore assume that the crevasse grow to 20 m instantly after its opening. In our results, the crevasse grow to 60–70 m after only 0.01 yr due to viscous deformation. Beyond the crevasse initiation process, the LEFM theory has been used successfully to model crevasse propagation (van der Veen, 1998a,b), rift propagation (Larour et al., 2004a,b), and calving (Krug et al., 2014) in prior studies.

In terms of time step, the LEFM model is called every 0.01 yr because the time scale of calving events is on the order of days to weeks (James et al., 2014; Murray et al., 2015). We investigated the impact of the time step by running the same experiment but calling the LEFM model every 0.005 yr for 0.15 yr (to save computational time and as the crevasse depth is stable after 0.15 yr). As shown in Fig. 1 below, the differences in crevasse depth are less than 20 m in all the experiments. The time step chosen for the LEFM therefore has no significant impact on the results. The limitations of this combination is now discussed in the manuscript at page 7 line 16–25 and the choose of time step is discussed at page 7, line 8–10. The figure is added to the supplementary material as Fig. S1.

2. Previous studies have found that one of the main issues with applying LEFM is the requirement of sizable pre-existing fractures (Nath and Vaughan 2003, Krug et al. 2014). Here, on the other hand, crevasses can be initiated from infinitesimal cracks. Firstly, an explanation regarding the model features (in contrast to previous studies) that allow for

such spontaneous initiations seems in order. Krug et al. (2014), for example, need to invoke a damage mechanics framework to "initiate" cracks. Highlighting differences and similarities between the present model and that of Krug et al. (2014) who also combine a Stokes model with LEFM - would be informative. Secondly, I must be misunderstanding something, because, if there's no initial threshold, it appears to me that this micro crack initiation would lead instantly to new crevasses wherever K>Kc? I understand that the authors are interested in the propagation, rather than initiation, of individual crevasses, but it seems that a physically plausible initiation process should be discussed in some form. Would a more complete model experiment initiate one crevasse at the location of maximum K, which then results in stress release in the vicinity, or similar?

Agreed. As mentioned above, with LEFM, the criterion $K > K_c$ is never satisfied when the crevasse depth is small (cm scale). A minimum depth is therefore required. Here, we start from an infinitesimal crevasse (always present) and assume that the crevasse can propagate if its required depth is smaller than 1 m. The reason we place the initial crevasse at different locations is to see how the propagation varies as a function of distance to the grounding line. This is now discussed in the manuscript at page 7, line 16–20.

We do not attempt to predict the initial crevasse location, for instance based on the initial K value. Radar echograms also indicate that crevasses are densely distributed on the ice shelf of Thwaites.

In Krug et al. (2014), damage mechanics is used to determine where a crevasse grows, but they do not discuss the crevasse propagation process. Their crevasses will only propagate if they penetrate the whole ice thickness to create a calving event. Here, we focus entirely on the propagation of crevasses. This is now pointed out in the manuscript at page 2, line 17–19.

3. In the abstract, the authors state that they "find that FS/LEFM produces surface and bottom crevasses that match the distribution of [observed] crevasse depth and width". Although the text mentions some ball-park numbers for the different observed and modeled crevasse depths and widths, a more direct comparison is missing. I believe it would be helpful to add a figure that shows such a direct comparison, e.g, a width-vs-height scatterplot for observed and modeled crevasses, color coded by the different model experiments (or maybe some other, more suitable, illustration). It would also be interesting to see how observed and modeled crevasses compare as a function of distance from the grounding line.

A width-vs-height scatter plot has been added in the manuscript (Fig. 7). The depth of the observed and modeled crevasses match well. Some observed crevasses are wider than our modeled crevasses because: 1) at the end of our experiments, the crevasse depth is stable but the width is still increasing, hence our model stops too soon; and 2) ocean forcing is

not included in the model, which could affect crevasse growth. This discussion of the figure is added in the manuscript at page 10, line 23–25.

4. One of the key points of this study is that the HO and SSA approximations fail since, for these approximations, the stress intensity factor, K, does not surpass the fracture toughness beyond a limited crevasse depth. This is traced back to the hydrostatic assumption necessary for HO and SSA. It would be helpful to actually show a figure of how K(t,x) evolves for the different models and different crevasse locations, and compare this to Kc. This may also help explain why "spontaneous" crevassing can occur in the model. It may even be worthwhile to show how the longitudinal stress, and ice and water pressure terms in (19) evolve. I was surprised to read that the crevasses in the HO and SSA simulations grew at all in the first place, and why are they then confined to a limit depth of 50 m? Maybe some further analysis of the evolution of K and a figure or two along the lines suggested above could help in the interpretation?

Agreed. We have now added a figure in the manuscript (Fig. 8) to show the relationship between K and crevasse depth with different models, different initial crevasse positions and different time. Crevasses never propagate in HO and SSA if the initial crevasse position is >2000 m downstream of grounding line. In these cases, the temporal changes in K are small because the geometry and thus the velocity and stress field do not change significantly. When the initial crevasse positions are within 2000 m of the grounding line, the crevasses propagate. Then, K decreases, the crevasses stop propagating and close up because of viscous flow. We think 50 m is only a limit for our specific flowline. It may vary for a different glacier with a different stress regime. This discussion of the figure is added in the manuscript at page 9, line 22–25.

Minor Comments

page 1

l 24. "iceberg calving will rise, which will" replace with "is likely to rise, which would"? (This may not be as certain as the current version implies.)

Done. The manuscript is modified at page 1, line 24.

page 2

l 7. "each process" which process? replace with "...the role of the different processes involved ..." ?

Done. The manuscript is modified at page 2, line 6–8.

l 8. "where crevasses propagate"

Done. The manuscript is modified at page 2, line 9.

l 11. change to "... it is necessary to use a fracture theory, such as LEFM"? (There may be other ways; currently it sounds like this is the one and only)

Done. The manuscript is modified at page 2, line 14.

page 3

Sec 2.2: It may be helpful to point out that (almost?) the same equations apply for the grounded and floating ice - only the boundary conditions differ.

Done. The manuscript is modified at page 3, line 19–20.

l 20. "values"

Done. The manuscript is modified at page 3, line 27.

l 26. add a reference for the 2D Full-Stokes model

Done. The manuscript is modified at page 4, line 6.

page 5

l 3. in previous work, (14) contains a N (pressure) factor. What happened to that?

Many sliding laws have been proposed in the past. Studies have shown that a Weertman sliding law (basal drag is non-linearly related to ice velocity) or a sliding law using a N factor (effective pressure at the bed) may be more appropriate than a linear sliding law in simulating glacier dynamics (Lliboutry, 1987; Cuffey and Paterson, 2010). Here, however, the time step and total simulation time are short. The grounding line does not migrate and the changes in ice thickness are small, so the influence of the particular sliding law we use is limited. After the inversion, the modeled velocity matches the observed velocity well and the background velocity field does not change significantly during the simulations. We therefore choose to use the linear sliding law for simplicity. This is now discussed in manuscript at page 5, line 13–17.

l 9. is $z_b(t)$ only unknown in FS, but not in HO an SSA?

In FS, if we do not use a dampening term, the vertical velocity becomes unrealistically high ($\sim 10^5$ m/yr) and destabilizes the system. In HO and SSA, $z_b(t)$ is not an unknown because we solve for ice thickness and use hydrostatic equilibrium to calculate the ice surface and bottom elevation. In these cases, the vertical velocity is decoupled from the system. Hence no dampening term is needed for HO and SSA. This is now discussed in the manuscript in page 5, line 26–27.

l 15. it is really the "ice-bedrock-ocean boundary"

Done. The manuscript is modified at page 5, line 29.

l 17. "migration of the grounding line"

Done. The manuscript is modified at page 6, line 2.

l 28. "avoids", or maybe better: "...term, invoked to avoid ..."

Done. The manuscript is modified at page 6, line 13.

page 6

l.7 it's worth mentioning that K and the stresses depend on time and x (not just z)

Done. The manuscript is modified at page 6, line 19.

l. 11 "equal"

Done. The manuscript is modified at page 6, line 26.

l.16 how is the width of the crevasse determined?

The crevasse is assumed to grow to 20 m wide once it opens. Then it becomes wider due to the viscous flow. This is now mentioned in the manuscript at page 7, line 4–5.

l.18 a discussion of the coupling scheme between FS and LEFM model would be of interest here (see Major Point 1)

We added a paragraph in section 2.5 (page 7, line 16–25) discussing the limitation of the combination of LEFM and viscous flow, namely the requirement of a minimum crevasse

depth and the difference in the scale between a crevasse modeled using LEFM and using viscous flow.

Sec 3.1. "FS model validation" rather than evaluation (?) (see also l.26)

Done. The manuscript is modified at page 7, line 27 and line 30.

l. 27 "migration of the grounding line"

Done. The manuscript is modified at page 7, line 31.

page 7

3.2. Model Setup: what's the duration of the integrations?

The duration is 0.3 yr. This is now added in the manuscript at page 8, line 11–12.

l. 1,2 "... to within X km"

Done. The manuscript is modified at page 8, line 3 and line 4.

l. 9 "In all ~~the~~ following experiments ..."

Done. The manuscript is modified at page 8, line 12.

l.12 These are not really "micro" crevasses, but rather "infinitesimal" crevasses, no? Although the latter is of course more cumbersome to use.

Done. The term "micro crevasses" is changed to "infinitesimal crevasses" throughout the paper.

l.13 I found the choice of initial crevasse positions somewhat surprising. I presume the high density of crevasse locations near the grounding line was initially motivated to better resolve the potentially more variable crevasse dynamics in this region? It might be worth justifying this choice with half a sentence. Otherwise, I'd believe a linear or logarithmic spacing throughout the shelf may have made more sense.

This is correct. The stress field is complex and exhibits large variations near the grounding line and this is why we choose the initial crevasse positions more densely in the grounding line region. This is now pointed out in the manuscript at page 8, line 18–20.

l.14 The "respectively" doesn't really work here. Maybe something like "In these experiments, the numbers 1-7 indicate crevasses initiated near the grounding line (at distances x = 0.5, ..., 3.5km from the grounding line); the numbers 8, 9 indicate crevasses in the middle of the ice shelf (x = 18, 28 km); and numbers 10, 11 indicate crevasses near the ice front (x = 35, 36 km).

Done. The manuscript is modified at page 8, line 16–18.

l.21 "...positions for Experiments D and E are ..."

Done. The manuscript is modified at page 8, line 26.

page 8

Sec 4.2. related to Major Comment 2: it would be nice to have some more information about the observed crevasses, i.e., how many, what's the spread, etc. I believe this could be summarized in a figure as suggested above.

The figure is added to the manuscript as Fig. 7.

l.11 Can the authors elaborate on why the ice is "tens of meters below equilibrium" near the grounding line?

This displacement below hydrostatic equilibrium is caused by a bending moment of the ice that is resulted from the abrupt change in basal conditions at the grounding line. This is now pointed out in the manuscript at page 9, line 14–15.

page 9

l. 5 (However, undercutting presumably occurs due to sustained ocean melt, i.e., it's not usually the case that undercutting occurs as a one-off sudden event, which then relaxes back to its normal state, but rather is maintained by a long-term temperature gradient in the water. So a fixed undercut profile might be more realistic.)

We run the undercutting experiments again by adding a 3000 m/yr basal melting in the undercutting region to achieve an almost fixed undercutting shape during the simulations. The results are shown in Fig.2 below. The results is similar to our previous in terms of crevasse depth and whether calving happens. If the high melt cannot sustain, the undercutting front diminishes in ∼0.1 yr. If the high melt can sustain, which is dependent on the seasonal variability of the ocean conditions, then the undercutting shape can sustain for a longer time. This is now discussed in the manuscript at page 12, line 1–3.

l. 16 equation (20) not (19), same for l. 17

Done. The manuscript is modified at page 10, line 27 and line 28.

l. 20 "... grounding line region stop ..."

Done. The manuscript is modified at page 10, line 31.

Paragraph starting l.24: this is where a figure of the stresses depending on the model, experiment, and crevasse depth/shape would be insightful

The figure is added to the manuscript as Fig. 8.

l. 26 "crevasses"

Done. The manuscript is modified at page 11, line 5.

page 11

l. 4 "crevasses"

Done. The manuscript is modified at page 12, line 21.

Figures

2. the blue lines are hard to see on my print version – choose green instead? also differentiate the two red lines somehow more clearly?

Done. Figure 2 is modified at page 18. We changed the blue lines to yellow lines and the lower red lines to green lines. The grounding line positions are now marked using cyan dots.

3. annotation: the β in the equation for bed drag should be α^2 (or $\alpha^2 N$?) caption: "... red line is the hydrostatic bottom elevation calculated ..."

Done. Figure 3 is modified at page 19.

5. color code the lines in (b) and the corresponding dots in (a), and then use different symbols for Elmer/Ice and ISSM? Or at least put numbers onto the profiles in (b). Also:

in a dynamical systems context, the unstable equilibrium state for the analytical solution (i.e. the negatively sloped part of the black curve) is commonly given as a dashed line

caption: something seems to have gone wrong with the parentheses around the references

Done. Figure 5 is modified at page 20.

6. Why does the FS friction coefficient suddenly become large again at 0 (yellow line overlaying the black box line)?

One node after the grounding line was mistakenly plotted with a default value, which was never used since it is floating. Figure 6 is now fixed at page 20. Thank you for pointing this out.

7. There is this interesting behavior that the crack height for profiles 8-11 seems to undergo a non-monotonic evolution, where it first jumps to a high value, then decreases for a bit, before it recovers to a value similar to the original one. Can the authors comment on that? Maybe a further analysis of the stresses as suggested above may help with this interpretation as well?

When the crevasses propagate, K will decrease. In profiles 1–4, the crevasses can continue to propagate after this decrease so they show a monotonic evolution through the simulation. In profile 5–11, however, the crevasses cannot continue to propagate after this decrease. Then, when the crevasses become shallower from viscous deformation, K increases until the crevasse can grow again. This is now mentioned in the manuscript at page 10, line 16–19.

Give it a title "Experiment A" and similarly for the panels of Figure 8 (to facilitate an easy comparison with the text/ captions)

caption: "... b) Details"

Done. Figure 9 (previous figure 7) is modified at page 22.

2 Response to Reviewer Jeremy Bassis

Detailed below are our point-by-point responses to the comments of Reviewer Jeremy Bassis. Reviewer comments are printed in blue font followed by our responses in black.

This study seeks to simulate surface and basal crevasse propagation using a variety of viscous models in an attempt to better understand the processes responsible for iceberg calving. The authors find that extra bending stresses near the grounding line that are resolved in full Stokes models are needed to accurately simulate the penetration depth of basal and surface crevasses. Moreover, the authors find that simulated crevasses are qualitatively similar to observed crevasses. Overall, I think this study is both interesting and novel and highly appropriate for publication in Cryosphere Discussion. I do, however, have two major points of concern along with a few more specific comments.

The first comment relates to the overarching goal of this study, which is presumably to better simulate iceberg calving. Here, I would like to see the authors make more detailed comparisons between observations and model predictions at the macro and local scale. For instance, the authors have strong conclusions about the role of different models in simulating crevasse penetration depths in Thwaites Glacier. But I had a hard time deciphering how well any of the models is able to reproduce the current ice tongue length of Thwaites. If the full Stokes model is able to accurately simulate the length of Thwaites Glacier tongue then this should be noted and celebrated. If the models have large discrepancies than, in the interest of honesty, this should also be acknowledged and discussed in light of (possible) missing processes.

We do not attempt to predict the length of the ice tongue with any of the models. First, we do not have a process to determine where the crevasse initiates. We choose its position arbitrarily to study how crevasses propagate at different locations. Second, the length of the ice tongue depends on many other factors, such as ocean currents (which slowly rotate the tongue to the west), the ice melange, buttressing from the sides, etc. We could predict the length of the ice tongue by using damage mechanics or subcritical crevasse propagation (Krug et al., 2014; Weiss, 2004), but this is beyond the scope of this study. Elements of this discussion are now added at page 12, line 14–17 as future work. Thank you for the comment.

Similarly, I would like to see the authors compare their simulated crevasse shapes with observed crevasse shapes (to the extent available). I realize that the radar probably doesn't fully resolve crevasse shapes, but one might be able to examine (at least to first order) penetration height and aspect ratios. Any such comparison would strengthen quantitative links between the model and observations, especially given the authors hints that such comparisons are positive.

A width-vs-height scatterplot for observed and modeled crevasses is added in the manuscript as Fig. 7. The depth of observed and modeled crevasses match well. Some observed crevasses are wider than our modeled crevasse width because: 1) at the end of our experiments, the crevasse depth is stable but the width is still increasing, hence our model stops

too soon; and 2) ocean forcing is not included in the model, which could affect crevasse growth. This discussion of the figure is added in the manuscript at page 10, line 23–25.

My second comment focuses on the methodology and, more specifically, the description of the methodology. To start, it is not obvious to me why stresses computed using a viscous model can be used to drive an elastic fracture mechanics model. Here the authors could assist readers by summarizing the tenets of the theory that they are using to map viscous to elastic stresses or by computing elastic stresses and comparing them to viscous stresses. My uncertainty in the method goes a bit deeper here, both in the physical model posed and the numerical implementation. I will start by describing the questions I have about the physical model before outlining some more numerical concerns. None of these issues are fatal, but point towards a need for a more thorough description of the model assumptions and implementation.

Physical crevasse model description:

1. I think Equation (20) is wrong. If σ_{xx} is the longitudinal stress then why is an additional cryostatic stress added? I'm also not sure that it is permissible in an elastic model to merely add a water pressure to the walls either without considering the effect on the stress field in the elastic body, but more on that later. Note also that Van der Veen does his computations using resistive stresses, not longitudinal or deviatoric stresses. The typo in Equation (20) makes it unclear to me that this translation has been done appropriately.

This was a typo. The stress we used is the deviatoric stress: $\sigma'_{xx} = \sigma_{xx} + p$. The resistive stress used in van der Veen (1998b) is described in van der Veen and Whillans (1989): $R_{xx} = \sigma_{xx} + L$, where R_{xx} is the resistive stress and $L = \rho g h$ is the lithostatic pressure. In the simulation, the calculated pressure p is only deviated from the lithostatic pressure by the order of 1%. Therefore, we do not think this difference has an impact on our results. The equation is now fixed at page 6, line 23.

2. The assumption of elasticity and water (or air) filling crevasses tells us exactly the shape of the crevasse. Perhaps this is already taken into account, but I had a hard time figuring out the initial condition. Formally, we know that for an elastic material, the width of the crack is related to the pressure on the walls through an integral relationship (see, e.g., Equation 2.1 in Self-Similar Solutions for Elastohydrodynamic Cavity Flow by D. A. Spence and P. Sharp Proceedings of the Royal Society). Water pressure only enters into this equation through the expression for the water pressure on the crack walls. For a narrow aspect ratio crack (width to height), we can make the lubrication theory approximation, whence an equation for crack width (or rate of change for crack width) can be found. See for example, Lister (1990, Buoyancy-driven fluid fracture : similarity solutions for the horizontal and vertical propagation of fluid-filled cracks). Of course the water can also freeze on the walls, but I don't think the authors are dealing with thermodynamics.

*3. Building on the previous point, the crevasse aspect ratio can be estimated by examining the ratio of pressure opening a crevasse to Young's modulus. For a 1 MPa stress opening a crevasse (an overestimate) and a typical 1-10 GPa Young's modulus I find that the aspect ratio of the crevasse is 0.0001-0.001. This translates into maximum crevasse widths (initially) that are of the order of ∼1 cm. For more typical stresses of the order of 100 kPa, I find initial widths of the order of a few mm. As a crude guess, one could take elliptical crevasses and evolve these, which is what I'm guessing the authors have done here, but this would seem to be incompatible with the 5 m resolution near the crevasses! More significantly, it shows that the crevasses the authors are considering (>200 m width) are **incompatible** with linear elastic fracture mechanics. Outside of the initial condition, I'm not convinced that LEFM is compatible with the fractures simulated. Of course, one might argue that new fractures are initiated at the tips of old fractures and the new fractures are elastic, but this needs to be made explicit.*

Since both points 2 and 3 concern the crevasse width, we combined our response. The width of the crevasses estimated from LEFM is ∼1 cm. However, once the crevasses are formed elastically, their shape is controlled by viscous flow, which grows the crevasses wider. Numerically, we cannot afford to run simulations with a mesh resolution of 1 cm. We therefore assume that the crevasses grow to 20 m wide after initiation. In the end, the crevasses grow from 20 to 60-70 m wide in 0.01 yr, so we think that it is reasonable to expect that the initial crevasse to grow to 20 m wide rapidly. When the LEFM method is employed again, we do not consider pre-existing crevasses because their width violate the assumption of LEFM. The pre-existing crevasses are only considered to be a feature of the ice shelf and affect stress field computed from the viscous model. The LEFM method is applied to an infinitesimal crevasse at the apex of the pre-existing crevasses. This new crevasse is opened to 20 m instantly and then it merges into the pre-existing crevasses due to viscous flow. This is now discussed in the manuscript from page 7, line 10–14 and line 20–25.

4. These issues aside, even in the most simple LEFM implementations, we start with a starter crack. What size starter cracks is assumed?

When using the LEFM, as mentioned above, the criterion K > Kc is never satisfied when the crevasse depth is small (cm scale) and a minimum required crevasse depth is needed. Here, we start from an infinitesimal crevasse (always present) and assume that the crevasse can propagate if its required depth is smaller than 1 m. This is now discussed in the manuscript at page 7, line 16–20.

Physical model implementation:

1. How are the crevasse implemented in ISSM? From the Figures I get the impression

that crevasses are merely tracers and nodes are not actually removed when propagating crevasses. This needs to be better explained

Once the crevasse depth is computed using LEFM, we change the surface and bottom elevation of the flowline to represent the crevasse propagation. Numerically, this is done by migrating the nodes vertically. In the entire simulation, none of the node is removed from the mesh. This is now mentioned in the manuscript at page 7, line 6–7.

2. If crevasse are implemented as tracers then they have no effect on the stress/strain rate field and this is probably fine for narrow crevasses, but is increasingly problematic for wide crevasses. We simulated crevasse evolution in Bassis and Ma (2015, 10.1016/j.epsl.2014.11.003) using an analytic calculation perturbation theory and found similar results to those shown, but found that the interaction between crevasses and the background strain rate was crucial to crevasse growth. This is particularly true for wide crevasses, which can result in accelerated flow into crevasses "healing" them. (We also found that large basal melt rates might erode basal crevasses, but this is more speculative.) More details are needed to assist readers to understand how the crevasses are initiated and evolved numerically. If this is a purely Lagrangian method, then this needs to be explained. If nodes are removed then this also should be explained. (There are thermodynamic and numerical issues associated with node removal, so these should be discussed if node removal is done.)

With the modified geometry after the crevasse shape is computed, the initial conditions of the viscous model are modified and thus the stress field is modified. The "healing" effect is also observed in our experiments as the crevasses become shallower and wider. This mentioned in the manuscript at page 7, line 5–8.

Technical comments:

Page 2, Line 10: The Nye zero stress model doesn't necessarily underestimate the stress-concentration at the tip of crevasses. In fact, as Weertman and others have shown, the Nye zero stress model corresponds to the LEFM problem of closely spaced crevasses. Moreover, even for isolated crevasses, ice behaves like a viscous fluid over long time scales. Hence, it is unclear to me that crevasses should have a stress concentration that is equivalent to that in an elastic plate. In other words, it is unclear to me why the Nye zero stress model isn't the more physically accurate model over long time scales and/or for closely spaced crevasses.

We agree that the Nye zero stress model is similar to LEFM with closely spaced crevasses. However, it has been shown that closely spaced crevasses will produce shallower crevasses than isolated crevasses (van der Veen, 1998b). Over a long time scale, there will not be any stress concentration in ice, but on a short time scale, especially when the crevasse

propagates, stress concentration exists at the tip of crevasses. This is discussed in the manuscript at page 2, line 11-13.

Page 2, Line 25: Here the authors should comment on the appropriateness of a flowline model that neglects lateral drag. What width are the authors using for the flowline (or are they assuming the width is infinite)?

The lateral drag is parameterized following Gagliardini et al. (2010). The width of the glacier is assumed to be 130 km from observations. This is described in the manuscript from page 4, line 27 to page 5, line 1.

Page 3, Line 5: I don't understand the need for a damping term in the full Stokes equations. The buoyancy term on the bottom acts like a spring and, I thought, the solution, then includes the additional degree of freedom z_b?

The dampening term is used to stabilize the model. Without this dampening term, the vertical velocity computed from FS model becomes unrealistically high ($\sim 10^5$ m/yr) and destabilizes the system. In HO and SSA, $z_b(t)$ is not an unknown because we solve for ice thickness and use hydrostatic equilibrium to calculate the ice surface and bottom elevation. In these cases, the vertical velocity is decoupled from the system. Hence the dampening term is not needed for HO and SSA. The manuscript is modified at page 5, line 26-27.

Equation 14: What is the physical reason for a linear sliding law? I thought prior research by Ian Joughin for Pine Island suggested a Weertman or plastic sliding law was most appropriate and would have (naively) thought that similar laws would be most appropriate for Thwaites as well? I apologize if I'm mistaken about this.

Some prior studies have shown that a Weertman sliding law (basal drag is non-linearly related to the ice velocity) or a sliding law considering a N factor (effective pressure at the bed) may be more appropriate than a linear sliding law in simulating glacier dynamics (Lliboutry, 1987; Cuffey and Paterson, 2010). Here, however, the time step and total simulation time are short. The grounding line does not migrate and the changes in ice thickness are small, so the influence of the particular sliding law we use is limited. After the inversion, the modeled velocity matches the observed velocity well and the background velocity field does not change significantly during the simulations. Therefore, we choose to use the linear sliding law for simplicity. This is now discussed in manuscript at page 5, line 1317.

Page 8, line 20. So only crevasses wider than 200 m are considered, but these crevasses would already appear to violate the assumptions of the LEFM?

We only consider crevasses wider than 200 m because the depth and width of observed crevasses are not estimated so precisely from the radar echograms. For smaller crevasses, the estimation error is high and the uncertainties in shape is large. In our model, LEFM is only responsible for the propagation of crevasse; the change of crevasse width is controlled by the viscous deformation of ice. The manuscript is modified at page 9, line 6–7.

3 Response to Short Comment from Joe Todd

Nice study, just a minor point:

*At page 6, line 20, the authors state: "Calving is assumed to occur when either the surface or the bottom crevasse reaches sea level (Benn et al., 2007)". Calving when surface crevasses reach the waterline is justified by the resultant hydrofracturing. Why do the authors choose to prescribe calving when basal crevasses reach the waterline? I think it should be made clearer that this is a *modification* of the crevasse depth criterion proposed by Benn et al. (2007) and Nick et al. (2010).*

This is a good point. The calving criterion of bottom crevasses has been changed. Now, calving only occurs when the bottom crevasse meets the surface crevasse or when the surface crevasse reaches sea level. This does not affect our results. In our experiments, every calving case except Exp. D2 and Exp. D3 has a bottom crevasse that penetrate not only the waterline but also the ice surface. For Exp. D2 and Exp. D3, the experiments were rerun with this new calving criterion. Calving still occurs, only few time steps later. We modified the description of the calving criterion in the manuscript at page 7, line 14–15. Figure 10 (previously figure 8) is also modified using the results obtained with this calving criterion.

References

Benn, D. I., Warren, C. R., and Mottram, R. H.: Calving processes and the dynamics of calving glaciers, Earth Sci. Rev., 82, 143–179, doi:10.1016/j.earscirev.2007.02.002, 2007.

Cuffey, K. M. and Paterson, W. S. B.: The Physics of Glaciers, 4th Edition, Elsevier, Oxford, 2010.

Gagliardini, O., Durand, G., Zwinger, T., Hindmarsh, R. C. a., and Le Meur, E.: Coupling of ice-shelf melting and buttressing is a key process in ice-sheets dynamics, Geophys. Res. Lett., 37, 1–5, doi:10.1029/2010GL043334, 2010.

James, T. D., Murray, T., Selmes, N., Scharrer, K., and OLeary, M.: Buoyant flexure and basal crevassing in dynamic mass loss at Helheim Glacier, Nature Geoscience, 7, 593–596, doi:10.1038/ngeo2204, URL http://www.nature.com/doifinder/10.1038/ngeo2204, 2014.

Krug, J., Weiss, J., Gagliardini, O., and Durand, G.: Combining damage and fracture mechanics to model calving, The Cryosphere, 8, 2101–2117, doi:10.5194/tc-8-2101-2014, 2014.

Larour, E., Rignot, E., and Aubry, D.: Processes involved in the propagation of rifts near Hemmen Ice Rise, Ronne Ice Shelf, Antarctica, J. Glaciol., 50, 329–341, 2004a.

Larour, E., Rignot, E., and Aubry, D.: Modelling of rift propagation on Ronne Ice Shelf, Antarctica, and sensitivity to climate change, Geophys. Res. Lett., 31, 1–4, doi:10.1029/2004GL020077, 2004b.

Lliboutry, L.: Realistic yet simple bottom boundary condition for glaciers and ice sheet, J. Geophys. Res., 92, 9101–9109, doi:10.1029/JB092iB09p09101, 1987.

Murray, T., Nettles, M., Selmes, N., Cathles, L. M., Burton, J. C., James, T. D., Edwards, S., Martin, I., O'Farrell, T., Aspey, R., Rutt, I., and Bauge, T.: Reverse glacier motion during iceberg calving and the cause of glacial earthquakes, Science, pp. science.aab0460–, doi:10.1126/science.aab0460, URL http://www.sciencemag.org/content/early/2015/06/24/science.aab0460, 2015.

van der Veen, C. J.: Fracture mechanics approach to penetration of bottom crevasses on glaciers, Cold Reg. Sci. Technol., 27, 213–223, 1998a.

van der Veen, C. J.: Fracture mechanics approach to penetration of surface crevasses on glaciers, Cold Reg. Sci. Technol., 27, 31–47, 1998b.

van der Veen, C. J. and Whillans, I. M.: Force budget: I. Theory and numerical methods, J. Glaciol., 35, 53–60, 1989.

Weiss, J.: Subcritical crack propagation as a mechanism of crevasse formation and iceberg calving, 50, 109–115, 2004.

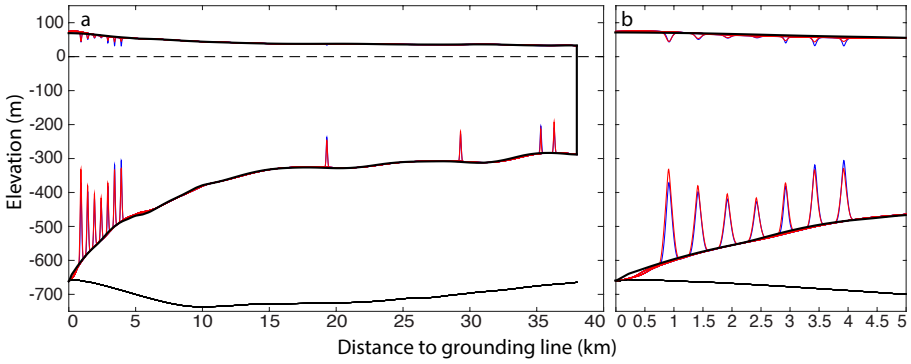

Figure 1: a) Crevasse propagation with different time steps. The blue lines are the shape of crevasses after 0.15 yr with the LEFM routine called every 0.01 yr. The red lines are the shape of the crevasses after 0.15 yr with the LEFM routine called every 0.005 yr. b) Zoom in to the grounding line region.

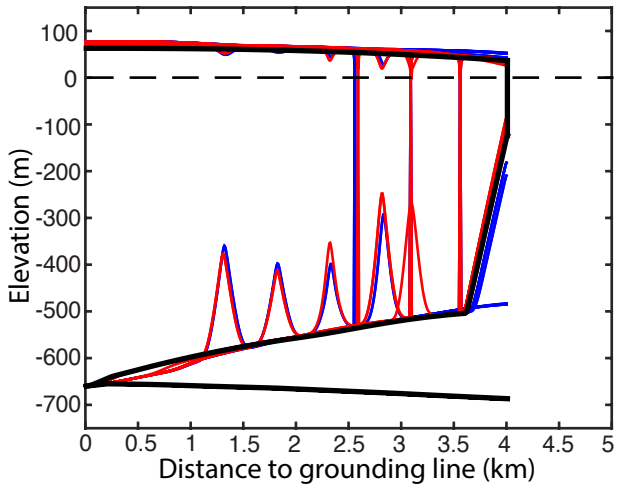

Figure 2: a) Crevasse propagation with undercutting. The blue lines are the shape of crevasses with no additional melt (Exp. E1–7). The red lines are the shape of the crevasses with 3000 m/yr additional melt the in undercutting region.

Iceberg calving of Thwaites Glacier, West Antarctica: Full-Stokes modeling combined with linear elastic fracture mechanics

Hongju Yu[1], Eric Rignot[1,2], Mathieu Morlighem[1], and Helene Seroussi[2]

[1]Department of Earth System Science, University of California, Irvine, Irvine, CA, USA
[2]Jet Propulsion Laboratory, California Institute of Technology, Pasadena, CA, USA

Correspondence to: Hongju Yu (hongjuy@uci.edu)

Abstract. Thwaites Glacier (TG), West Antarctica, has been losing mass and retreating rapidly in the past few decades. Here, we present a study of its calving dynamics combining a two-dimensional flowband Full Stokes (FS) model of its viscous flow with linear elastic fracture mechanics (LEFM) theory to model crevasse propagation and ice fracturing. We compare the results with those obtained with the higher-order (HO) and the shallow-shelf approximation (SSA) models coupled with LEFM. We find that FS/LEFM produces surface and bottom crevasses that match the distribution of crevasse depth and width observed from NASA's Operation IceBridge radar depth sounders, whereas HO/LEFM and SSA/LEFM do not generate crevasses that match observations. We attribute the difference to the non-hydrostatic condition of ice near the grounding line, which facilitates crevasse formation, and is accounted for by the FS model but not by the HO or SSA model. We also find that calving is enhanced when pre-existing surface crevasses are present, when the ice shelf is shortened or when the ice shelf front is undercut. The role of undercutting depends on the time scale of calving events. It is more prominent for glaciers with rapid calving rates than glaciers with slow calving rates. Glaciers extending into a shorter ice shelf are more vulnerable to calving than glaciers developing a long ice shelf, especially as the ice front retreats close to the grounding line region, which leads to a positive feedback. We conclude that the FS/LEFM combination yields substantial improvements in capturing the stress field near the grounding line for constraining crevasse formation and iceberg calving.

1 Introduction

Thwaites Glacier (TG) is the second largest and broadest ice stream in the Amundsen Sea Embayment (ASE) sector of West Antarctica (Fig. 1). Recent observations have reported significant thinning and retreat of this glacier (Rignot, 2001; Shepherd et al., 2002; Pritchard et al., 2009; Rignot et al., 2014). The mass balance of Thwaites was -34±16 Gt/yr in 2007 and this value has been decreasing until present to reach -50 Gt/yr in 2013 (Rignot, 2008; Shepherd et al., 2012; Mouginot et al., 2014). Its grounding line retreated 14 km from 1992 to 2011 (Rignot et al., 2014). The bed elevation of the vast majority of its drainage basin is well below sea level and decreases inland (Tinto and Bell, 2011; Rignot et al., 2014). Such a bed configuration makes the glacier unstable according to the marine ice sheet instability (MISI) theory (Weertman, 1974; Hughes, 1981; Schoof, 2007). With only a small ice shelf able to buttress it, TG may already be in a state of collapse (Parizek et al., 2013; Joughin et al., 2014). As the glacier retreats farther inland and loses its floating section, its rate of iceberg calving ~~will~~ is likely to rise, which

~~will~~ would increase the glacier's contribution to sea level rise (Deconto and Pollard, 2016). It is therefore essential to better understand and simulate the calving dynamics of TG.

Large calving events have been observed on the floating section of TG (Fig. 1b) by satellites (MacGregor et al., 2012). Densely distributed surface and especially bottom crevasses have been revealed by radar depth sounders on the ice (Fig. 2). As the buttressing ice shelf calves away and the grounding line retreats, the resistance to flow or buttressing force will decrease, which will favor further retreat and glacier speed up (MacGregor et al., 2012). The calving of icebergs is a difficult process to model because the ~~role of each process is unclear and a~~ physical mechanics of calving, such as the initiation, propagation and orientation of crevasses are unclear and direct observations are rare (Benn et al., 2007). A universal calving law is therefore missing. Most prior studies of crevasse propagation follow the work of Nye (1957), where ~~crevasse propagates~~ crevasses propagate based on the balance between longitudinal stress and ice overburden pressure (Bassis and Walker, 2012; Nick et al., 2013; Cook et al., 2014). Although this criterion helps reproduce ice front calving, it does not take into account the stress concentration at the rupture tips of crevasses~~and underestimates the depth of crevasses (Bassis and Walker, 2012; Plate et al., 2012)~~. This criterion corresponds to the case of multiple closely spaced crevasses (Weertman, 1973; Bassis and Walker, 2012; Ma et al., 2017), but it underestimates the penetration depth of isolated crevasses (van der Veen, 1998b; Plate et al., 2012). To simulate crevasse propagation at the rupture tip, it is necessary to use a fracture theory, such as the linear elastic fracture mechanics (LEFM)~~theory (van der Veen, 1998a, b; Larour et al., 2004b; Krug et al., 2014). In~~ . This theory has been successfully applied in prior studies. van der Veen (1998a, b) used LEFM to model penetration depth of surface and bottom crevasses. Larour et al. (2004a, b) employed LEFM along the rupture tips of ice shelves and showed that the modeled deformation around rupture tips match observations. Krug et al. (2014) combined LEFM with damage mechanics and reproduced the observed calving front position of Helheim Glacier in Greenland. In this study, however, the crevasse does not propagate unless it can propagate the whole ice thickness. In order to obtain a description of the stresses that control crevasse propagation in a time dependent fashion, ~~one~~ our approach is to model the viscous flow of the ice using an ice flow model and employ the LEFM theory for crevasse propagation.

In this work, we present a modeling study of the calving dynamics of TG using the Ice Sheet System Model (ISSM) (Larour et al., 2012) constrained by remote sensing observations. The model is conducted in two dimensions (2D) along a flowline, with geometry based on remote sensing observations. We combine various ice flow models with the LEFM theory to investigate crevasse propagation and iceberg calving. We compare the calving behavior of TG using different initial geometries and different levels of complexity of the numerical ice flow models used to calculate the stress field. We conclude on the importance of using FS for modeling the calving processes of TG and the conditions that are conducive to calving.

2 Data and Methods

2.1 Data

To model the glacier in 2D, we select a flowline at the center of the fast flowing region of TG as shown in Fig. 1. The flowline is 238 km long, with a 38 km long floating ice tongue (Fig. 3). BEDMAP-2 is used for ice surface, ice bottom and bed elevation (Fretwell et al., 2013). Over grounded ice, the bed elevation is replaced by the bed elevation computed from a mass

conservation method (Morlighem et al., 2011, 2013). At the grounding line, the two datasets display discrepancies in the order of hundreds of meters in a few places, but not along the particular flowline that we selected. The ice temperature field is the steady state temperature computed from the thermal model in ISSM (Larour et al., 2012; Seroussi et al., 2013). The thermal model is constrained by surface temperature from the regional atmospheric climate model RACMO2 (Lenaerts et al., 2012) and geothermal heat flux from Maule et al. (2005) and includes both conduction and advection processes (Morlighem et al., 2010; Seroussi et al., 2013). The ice surface velocity derived from interferometric synthetic aperture radar (InSAR) data collected in 2008 is also used to constrain our model (Rignot et al., 2011b).

The NASA Airborne Topographic Mapper (ATM) (Krabill, 2014) surface elevation data and the CReSIS MCoRDS ice thickness data (Gogineni, 2012) provide ice surface and ice shelf bottom elevation, respectively, along flight tracks. We use these observations to compare with our modeling results. Firn correction is applied to each flight track to ensure that the hydrostatic ice bottom calculated from surface elevation matches the observed ice bottom along the ice shelf. Fig. 2 shows the echograms of two flight tracks along the ice shelf of TG, superimposed by the bed picks from CReSIS, surface from ATM and the hydrostatic ice bottom calculated from these datasets.

2.2 Ice Flow Model

The simulations are performed on a 2D flowband model. The basic equations used in our simulations are summarized here for completeness. The ice is considered as an incompressible viscous material driven by gravity. The governing equations of this system are the conservation of momentum and mass:

$$\nabla \cdot \boldsymbol{\sigma} + \rho_i \boldsymbol{g} = \mathbf{0} \tag{1}$$

$$\nabla \cdot \boldsymbol{v} = 0 \tag{2}$$

where $\boldsymbol{\sigma}$ is the stress tensor, ρ_i the ice density, $\boldsymbol{g}$ the gravitational acceleration, and $\boldsymbol{v}$ the ice velocity. This governing equation is applied for both the grounded ice and the floating ice. The deformation of ice under stress is described by the constitutive law:

$$\boldsymbol{\sigma}' = 2\mu\dot{\boldsymbol{\varepsilon}} \tag{3}$$

where $\boldsymbol{\sigma}' = \boldsymbol{\sigma} + p\mathbf{I}$, is the deviatoric stress, p the ice pressure, $\mathbf{I}$ the identity matrix, μ the ice viscosity, and $\dot{\boldsymbol{\varepsilon}}$ the strain rate tensor. The ice viscosity μ is non-linear and follows Glen's law (Glen, 1955):

$$\mu = \frac{B}{2\dot{\varepsilon}_e^{\frac{n-1}{n}}} \tag{4}$$

where B is the ice viscosity parameter, $\dot{\varepsilon}_e$ the effective strain rate, and n the Glen's law exponent. Here, B is a function of ice temperature with ~~value~~ values interpolated from Cuffey and Paterson (2010) and the Glen's law exponent n is set to 3.

For a 2D flowband model, with (x, z) the horizontal and vertical directions, (u, w) the horizontal and vertical velocities, respectively, the above equations can be rewritten as:

$$\frac{\partial}{\partial x}\left(2\mu\frac{\partial u}{\partial x}\right)+\frac{\partial}{\partial z}\left(\mu\frac{\partial u}{\partial z}+\mu\frac{\partial w}{\partial x}\right)-\frac{\partial p}{\partial x}=0 \tag{5}$$

$$\frac{\partial}{\partial x}\left(\mu\frac{\partial u}{\partial z}+\mu\frac{\partial w}{\partial x}\right)+\frac{\partial}{\partial z}\left(2\mu\frac{\partial w}{\partial z}\right)-\frac{\partial p}{\partial z}-\rho_i g=0 \tag{6}$$

$$\frac{\partial u}{\partial x}+\frac{\partial w}{\partial z}=0 \tag{7}$$

This set of equations is the 2D Full-Stokes model and is computationally expensive (Larour et al., 2012). To reduce the computational cost, simplified models may be employed.

There are two widely used simplified models. The first one is the higher-order (HO) model (Blatter, 1995; Pattyn, 2003), which assumes that the horizontal gradient of vertical velocity and the bridging effect are negligible (van der Veen and Whillans, 1989). The governing equations are reduced to:

$$\frac{\partial}{\partial x}\left(4\mu\frac{\partial u}{\partial x}\right)+\frac{\partial}{\partial z}\left(\mu\frac{\partial u}{\partial z}\right)-\rho_i g\frac{\partial s}{\partial x}=0 \tag{8}$$

where s is the ice surface elevation. The vertical velocity w is decoupled from the system and is computed from incompressibility.

The second model is the Shallow-Shelf Approximation (SSA) model, which makes the additional assumption that the vertical shear is negligible (MacAyeal, 1989). This leads to the following 1D model:

$$\frac{\partial}{\partial x}\left(4H\bar{\mu}\frac{\partial u}{\partial x}\right)-\rho_i g H\frac{\partial s}{\partial x}=0 \tag{9}$$

where H is the ice thickness and $\bar{\mu}$ the depth-averaged viscosity.

At each time step, the geometry of the flowband is updated by a mass transport model~~using mass conservation~~. For FS, the ice surface and ice shelf bottom are treated as two independent free surfaces updated separately:

$$\frac{\partial z_j}{\partial t}+u_j\frac{\partial z_j}{\partial x}-w_j=\dot{m}_j \tag{10}$$

where the subscript j refers to either the ice surface $(j=s)$ or the ice shelf bottom $(j=b)$ and $\dot{m}_j$ is either the surface mass balance $(j=s)$ or the basal melt rate $(j=b)$. In HO and SSA, ~~only the ice thickness needs to be updated because the ice shelf is assumed to be in hydrostatic equilibrium~~ice surface and bottom elevations are not solved directly. Ice thickness is first solved through a mass transport model:

$$\frac{\partial H}{\partial t}+\nabla\cdot(H\bar{\boldsymbol{v}})=\dot{m}_s-\dot{m}_b \tag{11}$$

where $\bar{\boldsymbol{v}}$ is the depth-averaged velocity. The surface and bottom elevation of the ice shelf are then updated using hydrostatic equilibrium.

Lateral drag has to be parameterized in a flowband model. Here, it is represented by adding a body force on the ice shelf in the governing equation, as in Gagliardini et al. (2010):

$$f=-\frac{(n+1)^{\frac{1}{n}}B}{2^{\frac{1}{n}}W^{\frac{n+1}{n}}}\frac{2(n+1)^{\frac{1}{n}}B}{W^{\frac{n+1}{n}}}u^{\frac{1}{n}}; \tag{12}$$

where W is the width of glacier, taken here as 130 km. The convergence of ice from upstream to downstream also needs to be taken into account to conserve mass. Here, we first calculate the ice mass flux along the flowline. Then, we add an artificial surface mass balance term, $\dot{m}_a$, to the original surface mass balance, $\dot{m}_s$, to ensure that the ice mass flux is constant from the inflow boundary to the grounding line.

2.3 Boundary Conditions

At the ice surface, the atmospheric pressure exerted on ice is negligible and thus a stress free boundary condition is applied:

$$\boldsymbol{\sigma} \cdot \mathbf{n} = 0 \tag{13}$$

where $\mathbf{n}$ is the unit normal vector pointing outward.

At the bed, boundary conditions are different for grounded ice and floating ice. For grounded ice, the basal drag is assumed to follow a linear friction law:

$$\boldsymbol{\tau_b} = -\alpha^2 \boldsymbol{v}_b \tag{14}$$

where $\boldsymbol{\tau_b}$ is the basal drag, $\boldsymbol{v}_b$ the velocity tangential to the bed, and α the friction coefficient. Here, α is inferred from an inversion so that the modeled surface velocity matches observed surface velocity (Section 2.4). Other sliding laws have been proposed in the past, including a non-linear friction law (Weertman, 1957) and a friction law that includes effective pressure at the bed (Budd et al., 1979). In our simulations, the simulation time is short, the grounding line does not migrate, and the changes in ice thickness are small. The impact of the sliding law is therefore limited and we choose to use a linear sliding law for simplicity.

At the ice shelf bottom and the ice front, seawater pressure is applied at the ice-ocean boundary:

$$\boldsymbol{\sigma} \cdot \mathbf{n} = 0 \qquad z \geq 0 \tag{15}$$

$$\boldsymbol{\sigma} \cdot \mathbf{n} = \rho_w g z \, \mathbf{n} \qquad z < 0 \tag{16}$$

where ρ_w is the seawater density and sea level is at $z = 0$. In our simulations, the ice shelf bottom elevation, $z_b(t)$, is unknown when applying this boundary condition. A replacement with $z_b(t - dt)$, with dt the time step, produces large vertical velocities that destabilize the system (Durand et al., 2009a). ~~Therefore, a~~ A shelf dampening term based on ice velocity and geometry is therefore added to $z_b(t - dt)$ to approximate $z_b(t)$:

$$z_b(t) = z_b(t - dt) + \boldsymbol{v} \cdot \mathbf{n} \sqrt{1 + (\partial z_b(t - dt)/\partial x)^2} dt \tag{17}$$

For SSA and HO, z_b is not an unknown because we solve for ice thickness and use hydrostatic equilibrium to calculate the ice surface and bottom elevation. The dampening term is therefore not required.

The grounding line position is computed at every time step. For FS, it is treated as a contact problem (Nowicki and Wingham, 2008; Durand et al., 2009b; Drouet et al., 2013). At the ~~ice-bedrock~~ ice-bedrock-ocean boundary, the grounding line will retreat

if the water pressure is higher than the normal stress exerted by the ice. At the ice-ocean boundary, a non-penetration condition is imposed. For HO and SSA, the migration of the grounding line is determined by the hydrostatic equilibrium (Seroussi et al., 2014). At the inflow boundary, a Dirichlet boundary condition is applied for the velocity. The horizontal velocity is taken from InSAR-derived ice velocity data (Rignot et al., 2011b) and the vertical velocity is set to 0.

2.4 Inversion for Basal Friction

We have no direct observation of basal friction. In order to have a realistic representation of the basal conditions, we use an adjoint method as in Morlighem et al. (2010, 2013) to find a distribution of the basal friction coefficient, α, that minimizes a cost function:

$$\mathcal{J}(u,\alpha) = \int_{\Gamma_s} c_1 \frac{1}{2}(u-u_{obs})^2 d\Gamma + \int_{\Gamma_s} c_2 \frac{1}{2} \ln\left(\frac{|u|+\epsilon}{|u_{obs}|+\epsilon}\right)^2 d\Gamma + \int_{\Gamma_b} c_3 \frac{1}{2}\left(\frac{\partial \alpha}{\partial x}\right)^2 d\Gamma \tag{18}$$

where u is the modeled surface velocity, u_{obs} the observed surface velocity, ϵ a minimum value (10^{-8} m/yr) to avoid zero velocity, Γ_s and Γ_b the ice surface and bedrock, respectively. The first term of this cost function represents the misfit between modeled and observed velocity. The second term allows a better representation for slow flow regions and the third term is a Tikhonov regularization term~~that~~, invoked to avoid unphysical short scale spatial variations of α (Vogel, 2002). We calibrate c_1 and c_2 so that the first and second terms have the same order of magnitude and we calibrate c_3 using an L-curve analysis approach (Hansen, 2000).

2.5 Linear Elastic Fracture Mechanics Model

A physically-based LEFM model is used to simulate crevasse propagation. In the LEFM theory, there are three modes to open a crevasse: mode I opening, mode II sliding and mode III tearing. Only mode I is considered here. The key variables in LEFM are the stress intensity factor ~~K~~ $K(x,z,t)$ and the fracture toughness K_c. If K is larger than K_c, a crevasse will propagate. For a crevasse at a given location with a given stress field, K is computed through the integration of the normal stress from the bottom of the crevasse to the tip of the crevasse (van der Veen, 1998b). For bottom crevasses, the equations are:

$$K = \int_b^{b+h} \frac{2\sigma_n(z)}{\sqrt{\pi h}} G(z,h,H) dz \tag{19}$$

$$\sigma_n(z) = \sigma'_{xx}(z) + \rho_w g z - \rho_i g (s-z) \tag{20}$$

where h is the height between the tip and the bottom of the crevasse, b the elevation of the ice shelf bottom, H the ice thickness, σ_{xx} the longitudinal stress, and G a weighting function (Krug et al., 2014). For surface crevasses, the equations are similar with the water pressure term ~~equals~~ equal to zero since we assume no melt water production at the surface. K_c is a material property and previous studies showed that K_c ranges from 0.1 to 0.4 MPa m$^{1/2}$ for ice (Fischer et al., 1995; Rist et al., 1996, 2002). Here, K_c is set to 0.2 MPa m$^{1/2}$ following Krug et al. (2014).

A simple algorithm for the combination of ISSM and LEFM is described in Fig. 4. First, a position is chosen arbitrarily as the initial crevasse position. ISSM is used to calculate the stress field. With this stress field at the location of the initial crevasse, the LEFM theory is used to find the maximum heights of the surface and bottom crevasses that satisfy $K > K_c$. This process is assumed to be instant and the stress field is assumed to be unchanged (Duddu et al., 2013; Ma et al., 2017). Once the crevasse is opened, its width is assumed to grow to 20 m instantaneously (our mesh resolution is 5 m). The geometry is then updated to include the ~~propagation of these crevasses.~~ new crevasses. Numerically, this is done by migrating each node vertically, but none of the nodes is removed from the mesh. The new ice geometry is allowed to adjust viscously with ISSM for a period of 0.01 yr during which the crevasse becomes wider, shallower, and smoother due to the viscous deformation of ~~the ice. The LEFM model is then called againto test if the crevasses can still propagate at the center of the existing surface and bottom crevasses~~ice. This time step is chosen because the time scale of calving events is on the order of days to weeks (James et al., 2014; Murray et al., 2015) and a series of tests conducted with shorter time steps do not indicate any change in the results (Fig. S1). When the shape of a crevasse is adjusted viscously, its width violates LEFM assumptions. The pre-existing crevasse is therefore considered as a feature on the ice shelf and affects the stress field computed from the viscous model. When the LEFM is called again, it is applied to an infinitesimal crevasse at the apex of the pre-existing crevasse. The new crevasse, if it propagates, grows to 20 m wide instantly and then merges into the pre-existing crevasse through viscous deformation. Calving is assumed to occur when ~~either the surface or~~ the surface crevasse reaches sea level or when the bottom crevasse reaches ~~sea level (Benn et al., 2007).~~ the ice surface (Benn et al., 2007).

The limitations of our approach are as follows. The LEFM approach does not explain the propagation of a crevasse from 1 mm to 1 m scale (Weiss, 2004). The criterion $K < K_c$ is never satisfied when the crevasse depth is small (cm scale) and a minimum depth is required. Here, we assume that a crevasse can propagate if its minimum required depth is smaller than 1 m. The initiation of crevasses could be improved using a subcritical crevasse propagation method or damage mechanics (Weiss, 2004; Krug et al., 2014), but this is beyond the scope of our study. Another issue is associated with the width of crevasses, which should be ~1 cm according to LEFM (Lister, 1990; Bassis and Ma, 2015). Modeling a crevasse at this scale is computationally too demanding. Once a crevasse is formed, however, its shape is controlled by the viscous flow of ice, which reduces its depth and increases its width. In our experiments, crevasses are able to grow quickly from 20 m to 60-70 m in 0.01 yr when deforming under viscous flow. We therefore deem it reasonable to assume that the crevasses grow to a width of 20 m if LEFM shown that the infinitesimal crevasse can propagate.

3 Simulations

3.1 FS model ~~evaluation~~validation

ISSM is a coupled, thermo-mechanical, finite element, ice flow model (Larour et al., 2012). The three models, FS, HO and SSA are implemented in ISSM, which makes it practical to compare their performance (Morlighem et al., 2010; Seroussi et al., 2011). To ~~evaluate the FS model~~ validate the ability of the model to solve grounding line evolution with contact problem , we conduct the Experiment 3 of MISMIP, which is a model comparison experiment that evaluates the migration of the grounding

line in response to changes in ice rheology on an over-deepened bed (Pattyn et al., 2012). The ~~result~~results, shown in Fig. ~~5, indicates~~ 5, indicate that the grounding line is unstable on a retrograde bed and displays a hysteresis behavior in response to perturbations in ice rheology. This is consistent with the MISI theory, the analytical solution and other numerical models (Weertman, 1974; Schoof, 2007; Pattyn et al., 2012). The steady state grounding line positions obtained by ISSM agree with the FS solution obtained by Elmer/Ice (Durand et al., 2009a), to within 15 km. The results are also in good agreement with the analytical solution of Schoof (2007), especially in the retreating phase (step 7-13), to within 20 km. In the advancing phase, the difference is larger, ∼50 km. However, this level of discrepancy in grounding line position is considered to be satisfactory and has been attributed to numerical issues associated with mesh resolution (Durand et al., 2009a; Pattyn et al., 2012). ~~Therefore, we~~ We therefore conclude that ISSM is able to reproduce the results of MISMIP Exp 3.

3.2 Model Setup

In our simulations, the horizontal resolution of the mesh is 100 m, refined to 5 m within 3 km of the initial crevasse position. Vertically, the domain is uniformly discretized into 40 layers. In total, the domain has 281,680 elements. The time step we choose is 0.0005 yr (∼4.4 hr) and the LEFM model is called every 0.01 yr. ~~In all the~~ The simulations are run for 0.3 yr or until calving occurs, whichever happens first. In all following experiments, the basal melt rate is chosen so that the grounding line does not migrate and the ice shelf bottom has a stable elevation (within few meters).

Five sets of experiments, labeled Exp. A–E, are conducted to simulate the propagation of crevasses~~(Table ??)~~. In the first set, eleven experiments, Exp. A1–A11, are run with ~~micro~~ infinitesimal initial crevasses, zero crevasse depth and width, at both the surface and the bottom. In these experiments, the ~~number 1–11 indicates the initial crevasse position, respectively,~~ numbers 1–7 indicate crevasses initiated near the grounding line (at distances x = 0.5, 1, 1.5, 2, 2.5, 3, 3.5 ~~, 18, 28, 35 and 36~~ km downstream of the grounding line~~. These positions are chosen to represent, respectively, crevasse propagation near the grounding line,~~); the numbers 8 and 9 indicate crevasses initiated in the middle of the ice shelf ~~,~~ (x= 18, 28 km); and the numbers 10 and 11 indicate crevasses near the ice front ~~.~~ (x = 35, 36 km). The initial crevasses position are chosen more densely in the grounding line region as the stress conditions in this region are more complicated and exhibit more spatial variations.

In the next four sets of experiments, the initial glacier geometry is altered to evaluate its impact on crevasse propagation. The second (Exp. B1–B7) and the third (Exp. C1–C3) sets are designed to test the stability of TG with a shortened ice shelf. The length of the ice shelf is reduced from 38 to 4 km (Exp. B) and 2 km (Exp. C), respectively. In the fourth set of the experiments (Exp. D1–D7), a 3 m deep, 100 m wide initial surface crevasse is added to the initial geometry while the initial bottom crevasse is still kept as a ~~micro~~ infinitesimal crevasse. In the last set (Exp. E1–E7), we undercut the ice shelf front of a 4 km–long ice shelf by 400 m over the last 400 m. The initial crevasse positions for ~~these sets of experiments~~ experiments B-E are the same as Exp. A.

4 Results

4.1 Inversion

The inversion results of FS, HO and SSA are shown in Fig. ~~5~~6. For all three models, the inferred basal friction coefficient, α, has similar values and spatial patterns. The modeled ice surface velocities are in reasonable agreement. The modeled surface velocity after inversion closely matches the observed surface velocity over grounded ice. However, there remains a 200 m/yr, or 6%, difference in the grounding line region and on the ice shelf. We attribute this discrepancy to errors in ice rheology and uncertainties associated with the parameterization of the lateral drag.

4.2 Observed crevasses

In the data acquired by NASA ATM and CReSIS MCoRDS from 2009 to 2014 (Gogineni, 2012; Krabill, 2014), we find that surface and bottom crevasses are densely distributed on the ice shelf of TG (Fig. 1b and Fig. 2). With these data, we estimate the height and width of each surface and bottom crevasse (crevasses narrower than 200 m are neglected ~~).~~ because of the high uncertainties in their depth and width). The results are shown in Fig. 7. We find that the mean height is 18.7 m for surface crevasses and 103.1 m for bottom crevasses. The height of surface crevasse ranges from 2–82 m, but 90 % of them are within 2–40 m. The height of bottom crevasses ranges from 20–270 m. The mean width for surface and bottom crevasses are 821 m and 724 m, respectively, and 80 % of the crevasses have a width ranging from 300 m to 1000 m. The measurement error is 10 m for the ATM-derived ice surface elevation (Krabill, 2014) and 14 m for the MCoRDS-derived ice bottom elevation (Gogineni, 2012).

4.3 Non-hydrostatic behaviors

In the grounding line region~~of TG~~, i.e. within 5–10 km downstream of the grounding line, ~~the ice~~ ice is pushed down below hydrostatic equilibrium because of a bending moment applied on the ice as the basal regime changes abruptly across the grounding line. In TG, the ice is tens of meters below hydrostatic equilibrium (Fretwell et al., 2013). In our selected flowline, the maximum deviation is 85 m. In the two flight tracks shown in Fig. 2, we find ~~the maximum deviation to be~~ a maximum deviation of 130 m for track PQ and 122 m for track RS. In addition, in the ~~positions~~ region where surface and bottom crevasses ~~exist, this~~ are present, the deviation is larger ~~,~~ and measured in hundreds of meters (Fig. 2). In the FS solution~~of ISSM,~~ , it is possible to account for this non-hydrostatic condition~~can be simulated~~. For instance, we ~~get a maximum~~ obtain a maximum deviation of 68 m ~~deviation~~ in a steady state solution for our selected flowline.

4.4 Crevasse propagation

~~In all crevasse propagation experiments with~~ The evolution of K of selected experiments with different models is shown in Fig. 8. For HO and SSA, ~~we find that the height of a bottom crevasse never exceeds 50 m , which is small compared to observations~~the crevasses do not propagate if the initial crevasse position is >2000 m downstream of grounding line. When

the crevasse propagates, the stress intensity factor decreases. The crevasse then stops growing and closes up due to the viscous deformation. At the end of the simulations, the ~~crevasses never grow enough to produce a calving event.~~ bottom crevasse never exceeds 50 m, which is small compared to observations (Fig. 7). In other words, under the assumption of hydrostatic equilibrium, which is required ~~,~~ by HO and SSA~~are unable to grow crevasses that~~ , the crevasses cannot grow and generate calving events when combined with the LEFM theory. In the remainder of the study, we therefore only discuss the FS case.

In the first set of experiments (Exp. A1–A11), with the initial geometry and ~~micro~~ infinitesimal crevasses on the top and the bottom of the ice shelf, the crevasses of all eleven cases stop growing at the end of the simulations and none produce a calving event (Fig. 9). The final height of bottom crevasses is 200–300 m near the grounding line (Exp. A1–A7) and 50–100 m downstream (Exp. A8–A11). The surface crevasses are one order of magnitude smaller, 10–15 m near the grounding line and 2–5 m downstream. The width of all crevasses is between 400 and 500 m.

The results of the experiments with varying initial geometries are shown in Fig. 10. With an ice shelf shortened to 4 km, calving occurs within 1 km of the ice front (Exp. B6 and B7, Fig. 10a) and the other experiments (Exp. B1–B5) have results similar to the initial 38 km long ice shelf (Exp. A1–A5), i.e. the final bottom crevasse height does not exceed 200–300 m. With an ice shelf shortened to 2 km, calving occurs in all three experiments (Exp. C1–C3, Fig. 10b).

In Exp. D1–D7, where we add a 3 m deep, 100 m wide, initial surface crevasse, calving occurs for crevasses located within 1.5 km of the grounding line (Exp. D1–D3, Fig. 10c). Further downstream (Exp. D4–D7), the crevasse propagation is identical to the case with ~~micro~~ infinitesimal surface crevasses (Exp. A4–A7).

In the last set, where the ice shelf is shortened and undercut, we find that calving occurs within 1.5 km of the ice front (Exp. E5–E7, Fig. 10d). In regions where calving does not occur, undercutting vanishes slowly within 0.1 yr due to the viscous deformation and downstream advection of ice.

Among all experiments, only Exp. B6 produces calving caused by a surface crevasse propagating to sea level and it takes 0.24 yr for the calving to occur. For all other calving cases, calving occurs because a bottom crevasse propagates to sea level and the process is five times more rapid, i.e. within 0.05 yr. For the cases that calving does not take place, the crevasses stop growing before the end of the simulations. In Exp. A5–A11, the modeled crevasses undergo a non-monotonic evolution where the crevasses depth decreases in a few time steps during the simulation (Fig. 9). This evolution is caused by the temporal change in K. K decreases when the crevasse propagates until it stops grow. K then increases when the crevasse become shallower viscously until it can propagate again.

5 Discussion

The size of surface and bottom crevasses produced by our crevasse propagation experiments with FS ~~(Fig. 9)~~ are comparable with the sizes of surface and bottom crevasses observed by ice radar sounders (Fig. ~~2~~7). This suggests that the combination of FS with the LEFM theory is a realistic way to model crevasse propagation and iceberg calving. Some observed crevasses are wider than our modeled crevasses because the width of crevasse is still increasing at the end of our simulations (the depth is stable). Furthermore, we do not include ocean forcing in our model, which could affect crevasse growth. With HO and SSA,

however, because of the assumption of hydrostatic equilibrium, the water pressure term and the overburden ice pressure term in Eq. (~~19~~20) cancel each other at the bottom of the ice shelf and thus the bottom crevasses are unable to grow to a size that matches observations. With the non-hydrostatic condition included, the two pressure terms in Eq. (~~19~~20) do not cancel each other with FS in the region near the grounding line or the region with crevasses, which helps propagate the crevasses. In the radar echograms, large bottom crevasses (over 100 m) are also observed along the ice shelf, tens of kilometers downstream of the grounding line. According to our results from Exp. A, the crevasses formed in the grounding line region stop growing once they reach a stable size. Therefore, we posit that these crevasses are the result of advection of crevasses formed upstream. In summary, the non-hydrostatic condition plays a major role in crevasse formation. Not accounting for this condition makes it difficult to explain the observed crevasse pattern.

In our simulations, we find that crevasses propagate significantly faster near the ice front when the ice shelf is shortened. In principle, the length of a nearly non-confined ice shelf, such as the floating ice tongue of TG, should not have a major impact on the buttressing that the ice shelf exerts on grounded ice. Here, we find that the propagation of ~~crevasse~~ crevasses near the ice front, while limited for the initial 38 km-long ice shelf, becomes significantly enhanced with a shortened ice shelf. When the ice shelf is shortened, the longitudinal stress near the ice front increases at the surface and decreases at the bottom. The increase in the surface stress makes it easier for the surface crevasse to propagate, while the decrease in bottom stress prevents the propagation of the bottom crevasse. As time goes, the stress at the bottom increases and the surface crevasse grows. The bottom crevasse is then able to propagate quickly through the entire ice column to cause calving because of the large difference between the water pressure and the overburden ice pressure. If calving takes place and creates a shorter ice shelf, our model predicts that the new ice shelf will be more prone to calving, i.e. a positive feedback.

When an initial crevasse of 3 m depth and 100 m width is added to the surface, we find that the surface crevasse grows quickly to 35 m before the bottom crevasse starts to propagate. The large difference between the water pressure and the overburden ice pressure at the bottom however, makes the bottom crevasse propagate rapidly through the entire ice thickness and produces calving. This is consistent with Bassis and Walker (2012), who suggested that ice shelves are difficult to form in the presence of pre-existing crevasses. However, long ice shelves calving at the grounding line region is not something commonly observed on TG. Three reasons might explain this result. One reason is that we assume that a surface crevasse aligns perfectly with a ~~micro-crack~~ infinitesimal crevasse at the bottom, which is not certain. A second one is that bottom crevasses could also form from thermal cracking (Humbert and Steinhage, 2011; Vaughan et al., 2012), in particular not aligned with a surface ~~crack~~crevasse. Thermal cracking would facilitate the propagation of a bottom crevasse. If the corresponding surface crevasse remains shallow, the seawater-filled bottom crevasse formed by thermal cracking will not propagate far because the difference between the water pressure and the overburden ice pressure will be smaller than in the presence of a deep surface crevasse. The third reason is that most surface crevasses are formed in train, whereas here we only model one. A train of crevasses creates a shielding effect, which effectively reduces the stress concentration at rupture tips and anneals the propagation of crevasses (van der Veen, 1998b; Krug et al., 2014).

Undercutting on the ice front is a common feature, especially for tidewater glaciers with a short to non-existent floating section (Rignot et al., 2010). In a prior study, O'Leary and Christoffersen (2013) suggested that undercutting leads to signif-

icant changes in the stress field that enhances calving. Cook et al. (2014) argued, however, that the change in stress field is only significant in diagnostic simulations and is much smaller in prognostic simulations. Krug et al. (2015) also showed that undercutting has no effect on the glacier mass balance on annual time scales. Here, we find that undercutting does affect the stress field significantly near the ice front but its impact on calving depends on the time scale of calving events. Undercutting increases the surface stress and decreases the bottom stress just as in the case of a shorter ice shelf and thus induces a similar type of calving. The influence of the stress field is however time dependent due to the viscous adjustment of ice. In our simulations, we find that if the undercutting is not large enough to produce calving within about 0.1 yr, then it will have no impact on calving. If calving occurs on shorter time scales, then undercutting significantly enhances the process. The high melt that produces undercutting, however, is not considered in our simulation. If the high melt is sustained, which depends on the seasonal variability of thermal forcing from the ocean, the time scale of undercutting will be longer. This conclusion effectively reconciles the previous studies because it shows that the impact of undercutting depends on the time scale of calving events. We conclude that the impact of undercutting will be more significant for fast-moving glaciers with high calving rates than for slow moving glaciers with a low calving rate. A high calving rate will give less time for the glacier to adjust viscously to the undercutting than for a slow calving glacier. As a conjecture, since glaciers with a high calving rate have more impact on the total mass balance, we conclude that undercutting is an important factor in the study of calving dynamics.

In this study, the simulations are ~~all~~ conducted in a 2D flowband model with one crevasse propagation event. It would be of interest to generalize the present simulation to a 3D geometry with multiple crevasses and a moving ice front combining subcritical propagation or damage mechanics. In 3D, a better representation of the lateral shear and a complete surface/bed geometry will provide a more realistic context for the models. The simulation of a series of calving events with a train of crevasses over a long time period would provide more realistic information about how a glacier will respond to a calving event in terms of the migration of its grounding line and the evolution of its ice speed. Subcritical propagation or damage mechanics would help improve the simulation of the initial crevasse position and the initial processes that develop an infinitesimal crevasse into a $\sim$ 1 m deep crevasse (Weiss, 2004; Krug et al., 2014). With this additions, we would be in a position to try to project calving events.

6 Conclusions

We use a two-dimensional flowband Full-Stokes model coupled with LEFM theory to model the calving behavior of TG. We find that FS combined with LEFM produces crevasses consistent in width and depth with observations and ~~is capable of producing calving events~~produces calving events, whereas the HO and SSA models do not. The reason for the propagation of ~~crevasse~~ crevasses is the existence of a non-hydrostatic ~~conditions of ice near~~ condition of ice immediately downstream of the grounding line, which is not accounted for in simplified models that assume ~~hydrostatic conditions~~ a hydrostatic condition everywhere on the ice shelf. We also find that calving is enhanced in the presence of pre-existing surface crevasses, ~~on~~ shorter ice shelves~~and~~ , or if the ice front is undercut. We conclude that it is important to consider the full stress ~~field~~ regime of ice in the grounding line region to ~~properly represent the stress field and~~ replicate the conditions conducive to calving events,

especially the non-hydrostatic condition that is critical to propagate the crevasses. Further studies ought to examine how these results ~~may vary in a~~ vary in 3D ~~domain with complete modeling of~~ and including the role of ~~the~~ lateral margins.

Acknowledgements. This work was carried out at the University of California Irvine and at California Institute of Technology's Jet Propulsion Laboratory under a contract with the Cryosphere Science Program of the National Aeronautics and Space Administration, grant NNX14AN03G. We thank the reviewers T.Wagner, J. Bassis and J. Todd for their insightful and helpful comments.

References

Bassis, J. N. and Ma, Y.: Evolution of basal crevasses links ice shelf stability to ocean forcing, 409, 203–211, doi:10.1016/j.epsl.2014.11.003, 2015.

Bassis, J. N. and Walker, C. C.: Upper and lower limits on the stability of calving glaciers from the yield strength envelope of ice, Proceedings of the Royal Society A: Mathematical, Physical and Engineering Sciences, 468, 913–931, doi:10.1098/rspa.2011.0422, 2012.

Benn, D. I., Warren, C. R., and Mottram, R. H.: Calving processes and the dynamics of calving glaciers, Earth Sci. Rev., 82, 143–179, doi:10.1016/j.earscirev.2007.02.002, 2007.

Blatter, H.: Velocity And Stress-Fields In Grounded Glaciers: A Simple Algorithm For Including Deviatoric Stress Gradients, J. Glaciol., 41, 333–344, 1995.

Budd, W. F., Keage, P. L., and Blundy, N. A.: Empirical studies of ice sliding, J. Glaciol., 23, 157–170, 1979.

Cook, S., Rutt, I. C., Murray, T., Luckman, a., Zwinger, T., Selmes, N., Goldsack, a., and James, T. D.: Modelling environmental influences on calving at Helheim Glacier in eastern Greenland, Cryosphere, 8, 827–841, doi:10.5194/tc-8-827-2014, 2014.

Cuffey, K. M. and Paterson, W. S. B.: The Physics of Glaciers, 4th Edition, Elsevier, Oxford, 2010.

Deconto, R. M. and Pollard, D.: Contribution of Antarctica to past and future sea-level rise, Nature, 531, 591–597, doi:10.1038/nature17145, http://dx.doi.org/10.1038/nature17145, 2016.

Drouet, a. S., Docquier, D., Durand, G., Hindmarsh, R., Pattyn, F., Gagliardini, O., and Zwinger, T.: Grounding line transient response in marine ice sheet models, The Cryosphere, 7, 395–406, doi:10.5194/tc-7-395-2013, 2013.

Duddu, R., Bassis, J. N., and Waisman, H.: A numerical investigation of surface crevasse propagation in glaciers using nonlocal continuum damage mechanics, Geophys. Res. Lett., 40, doi:10.1002/grl.50602, 2013.

Durand, G., Gagliardini, O., de Fleurian, B., Zwinger, T., and Le Meur, E.: Marine ice sheet dynamics: Hysteresis and neutral equilibrium, J. Geophys. Res., 114, 1–10, doi:10.1029/2008JF001170, 2009a.

Durand, G., Gagliardini, O., Zwinger, T., Le Meur, E., and Hindmarsh, R. C. A.: Full Stokes modeling of marine ice sheets: influence of the grid size, Ann. Glaciol., 50, 109–114, 2009b.

Fischer, M. P., Alley, R. B., and Engelder, T.: Fracture toughness of ice and firn determined from the modified ring test, Journal of Glaciology, 41, 383–394, 1995.

Fretwell, P., Pritchard, H. D., Vaughan, D. G., Bamber, J. L., Barrand, N. E., Bell, R., Bianchi, C., Bingham, R. G., Blankenship, D. D., Casassa, G., Catania, G., Callens, D., Conway, H., Cook, a. J., Corr, H. F. J., Damaske, D., Damm, V., Ferraccioli, F., Forsberg, R., Fujita, S., Gim, Y., Gogineni, P., Griggs, J. a., Hindmarsh, R. C. a., Holmlund, P., Holt, J. W., Jacobel, R. W., Jenkins, A., Jokat, W., Jordan, T., King, E. C., Kohler, J., Krabill, W., Riger-Kusk, M., Langley, K. a., Leitchenkov, G., Leuschen, C., Luyendyk, B. P., Matsuoka, K., Mouginot, J., Nitsche, F. O., Nogi, Y., Nost, O. a., Popov, S. V., Rignot, E., Rippin, D. M., Rivera, A., Roberts, J., Ross, N., Siegert, M. J., Smith, a. M., Steinhage, D., Studinger, M., Sun, B., Tinto, B. K., Welch, B. C., Wilson, D., Young, D. a., Xiangbin, C., and Zirizzotti, A.: Bedmap2: improved ice bed, surface and thickness datasets for Antarctica, The Cryosphere, 7, 375–393, 2013.

Gagliardini, O., Durand, G., Zwinger, T., Hindmarsh, R. C. a., and Le Meur, E.: Coupling of ice-shelf melting and buttressing is a key process in ice-sheets dynamics, Geophys. Res. Lett., 37, 1–5, doi:10.1029/2010GL043334, 2010.

Glen, J. W.: The creep of polycrystalline ice, Proc. R. Soc. A, 228, 519–538, 1955.

Gogineni, P.: CReSIS Radar Depth Sounder Data, http://data.cresis.ku.edu/, 2012.

Hansen, P. C.: The L-Curve and its Use in the Numerical Treatment of Inverse Problems, in: in Computational Inverse Problems in Electrocardiology, ed. P. Johnston, Advances in Computational Bioengineering, pp. 119–142, WIT Press, Southampton, 2000.

Hughes, T.: The weak underbelly of the West Antarctic ice-Sheet, Journal of Glaciology, 27, 518–525, 1981.

Humbert, A. and Steinhage, D.: The evolution of the western rift area of the Fimbul Ice Shelf, Antarctica, The Cryosphere, 5, 931–944, doi:10.5194/tc-5-931-2011, http://www.the-cryosphere.net/5/931/2011/, 2011.

James, T. D., Murray, T., Selmes, N., Scharrer, K., and O'Leary, M.: Buoyant flexure and basal crevassing in dynamic mass loss at Helheim Glacier, Nature Geoscience, 7, 593–596, doi:10.1038/ngeo2204, http://www.nature.com/doifinder/10.1038/ngeo2204, 2014.

Joughin, I., Smith, B. E., and Medley, B.: Marine ice sheet collapse potentially under way for the Thwaites Glacier Basin, West Antarctica., Science (New York, N.Y.), 344, 735–8, doi:10.1126/science.1249055, 2014.

Krabill, W.: IceBridge ATM L2 Icessn Elevation, Slope, and Roughness, Version 2, 2014.

Krug, J., Weiss, J., Gagliardini, O., and Durand, G.: Combining damage and fracture mechanics to model calving, The Cryosphere, 8, 2101–2117, doi:10.5194/tc-8-2101-2014, 2014.

Krug, J., Durand, G., Gagliardini, O., and Weiss, J.: Modelling the impact of submarine frontal melting and ice mélange on glacier dynamics, The Cryosphere Discussions, 9, 183–221, doi:10.5194/tcd-9-183-2015, 2015.

Larour, E., Rignot, E., and Aubry, D.: Processes involved in the propagation of rifts near Hemmen Ice Rise, Ronne Ice Shelf, Antarctica, J. Glaciol., 50, 329–341, 2004a.

Larour, E., Rignot, E., and Aubry, D.: Modelling of rift propagation on Ronne Ice Shelf, Antarctica, and sensitivity to climate change, Geophys. Res. Lett., 31, 1–4, doi:10.1029/2004GL020077, 2004b.

Larour, E., Seroussi, H., Morlighem, M., and Rignot, E.: Continental scale, high order, high spatial resolution, ice sheet modeling using the Ice Sheet System Model (ISSM), J. Geophys. Res., 117, 1–20, doi:10.1029/2011JF002140, 2012.

Lenaerts, J. T. M., van den Broeke, M. R., van de Berg, W. J., van Meijgaard, E., Kuipers Munneke, P., and Munneke, P. K.: A new, high-resolution surface mass balance map of Antarctica (1979-2010) based on regional atmospheric climate modeling, Geophys. Res. Lett., 39, 1–5, doi:10.1029/2011GL050713, 2012.

Lister, J. R.: Buoyancy-driven fluid fracture : similarity solutions for the horizontal and vertical propagation of fluid-filled cracks, 217, 213–239, 1990.

Ma, Y., Tripathy, C. S., and Bassis, J. N.: Bounds on the calving cliff height of marine terminating glaciers, 44, 1–7, doi:10.1002/2016GL071560, 2017.

MacAyeal, D. R.: Large-scale ice flow over a viscous basal sediment: Theory and application to Ice Stream B, Antarctica, J. Geophys. Res., 94, 4071–4087, 1989.

MacGregor, J. A., Catania, G. A., Markowski, M. S., and Andrews, A. G.: Widespread rifting and retreat of ice-shelf margins in the eastern Amundsen Sea Embayment between 1972 and 2011, J. Glaciol., 58, 458–466, 2012.

Maule, C. F., Purucker, M. E., Olsen, N., and Mosegaard, K.: Heat Flux Anomalies in Antarctica Revealed by Satellite Magnetic Data, Science, 309, 464–467, 2005.

Morlighem, M., Rignot, E., Seroussi, H., Larour, E., Ben Dhia, H., and Aubry, D.: Spatial patterns of basal drag inferred using control methods from a full-Stokes and simpler models for Pine Island Glacier, West Antarctica, Geophysical Research Letters, 37, L14 502, 2010.

Morlighem, M., Rignot, E., Seroussi, H., Larour, E., Ben Dhia, H., and Aubry, D.: A mass conservation approach for mapping glacier ice thickness, Geophys. Res. Lett., 38, 1–6, doi:10.1029/2011GL048659, 2011.

Morlighem, M., Seroussi, H., Larour, E., and Rignot, E.: Inversion of basal friction in Antarctica using exact and incomplete adjoints of a higher-order model, J. Geophys. Res., 118, 1746–1753, doi:10.1002/jgrf.20125, 2013.

Mouginot, J., Rignot, E., and Scheuchl, B.: Sustained increase in ice discharge from the Amundsen Sea Embayment, West Antarctica, from 1973 to 2013, Geophys. Res. Lett., 41, 1–9, doi:10.1002/2013GL059069, 2014.

Murray, T., Nettles, M., Selmes, N., Cathles, L. M., Burton, J. C., James, T. D., Edwards, S., Martin, I., O'Farrell, T., Aspey, R., Rutt, I., and Bauge, T.: Reverse glacier motion during iceberg calving and the cause of glacial earthquakes, Science, pp. science.aab0460–, doi:10.1126/science.aab0460, http://www.sciencemag.org/content/early/2015/06/24/science.aab0460, 2015.

Nick, F. M., Vieli, A., Andersen, M. L., Joughin, I., Payne, A., Edwards, T. L., Pattyn, F., and van de Wal, R. S. W.: Future sea-level rise from Greenland's main outlet glaciers in a warming climate, Nature, 497, 235–238, 2013.

Nowicki, S. M. J. and Wingham, D. J.: Conditions for a steady ice sheet–ice shelf junction, Earth Planet. Sci. Lett., 265, 246–255, doi:10.1016/j.epsl.2007.10.018, 2008.

Nye, J. F.: The distribution of stress and velocity in glaciers and ice-sheets, Proc. R. Soc. A, 239, 113–133, 1957.

O'Leary, M. and Christoffersen, P.: Calving on tidewater glaciers amplified by submarine frontal melting, Cryosphere, 7, 119–128, doi:10.5194/tc-7-119-2013, 2013.

Parizek, B. R., Christianson, K., Anandakrishnan, S., Alley, R. B., Walker, R. T., Edwards, R. a., Wolfe, D. S., Bertini, G. T., Rinehart, S. K., Bindschadler, R. a., and Nowicki, S. M. J.: Dynamic (in)stability of Thwaites Glacier, West Antarctica, J. Geophys. Res., 118, 1–18, doi:10.1002/jgrf.20044, 2013.

Pattyn, F.: A new three-dimensional higher-order thermomechanical ice sheet model: Basic sensitivity, ice stream development, and ice flow across subglacial lakes, J. Geophys. Res., 108, 1–15, doi:10.1029/2002JB002329, 2003.

Pattyn, F., Schoof, C., Perichon, L., Hindmarsh, R. C. a., Bueler, E., de Fleurian, B., Durand, G., Gagliardini, O., Gladstone, R., Goldberg, D., Gudmundsson, G. H., Huybrechts, P., Lee, V., Nick, F. M., Payne, a. J., Pollard, D., Rybak, O., Saito, F., and Vieli, A.: Results of the Marine Ice Sheet Model Intercomparison Project, MISMIP, The Cryosphere, 6, 573–588, doi:10.5194/tc-6-573-2012, http://www.the-cryosphere.net/6/573/2012/, 2012.

Plate, C., Müller, R., Humbert, A., and Gross, D.: Evaluation of the criticality of cracks in ice shelves using finite element simulations, The Cryosphere, 6, 973–984, doi:10.5194/tc-6-973-2012, http://www.the-cryosphere.net/6/973/2012/, 2012.

Pritchard, H. D., Arthern, R. J., Vaughan, D. G., and Edwards, L. A.: Extensive dynamic thinning on the margins of the Greenland and Antarctic ice sheets, Nature, 461, 971–975, doi:10.1038/nature08471, 2009.

Rignot, E.: Evidence for rapid retreat and mass loss of Thwaites Glacier, West Antarctica, J. Glaciol., 47, 213–222, doi:10.3189/172756501781832340, 2001.

Rignot, E.: Changes in West Antarctic ice stream dynamics observed with ALOS PALSAR data, Geophys. Res. Lett., 35, 1–5, doi:10.1029/2008GL033365, 2008.

Rignot, E., Koppes, M., and Velicogna, I.: Rapid submarine melting of the calving faces of West Greenland glaciers, Nat. Geosci., 3, 187–191, doi:10.1038/NGEO765, 2010.

Rignot, E., Mouginot, J., and Scheuchl, B.: Antarctic grounding line mapping from differential satellite radar interferometry, Geophysical Research Letters, 38, n/a–n/a, doi:10.1029/2011GL047109, 2011a.

Rignot, E., Mouginot, J., and Scheuchl, B.: Ice Flow of the Antarctic Ice Sheet, Science, 333, 1427–1430, doi:10.1126/science.1208336, 2011b.

Rignot, E., Mouginot, J., Morlighem, M., Seroussi, H., and Scheuchl, B.: Widespread, rapid grounding line retreat of Pine Island, Thwaites, Smith and Kohler glaciers, West Antarctica from 1992 to 2011, Geophys. Res. Lett., in press, 2014.

Rist, M., Sammonds, P., Murrell, S., Meredith, P., Oerter, H., and Doake, C.: Experimental fracture and mechanical properties of Antarctic ice: preliminary results, Annals of Glaciology, 23, 284–292, 1996.

Rist, M. A., Sammonds, P. R., Oerter, H., and Doake, C. S. M.: Fracture of Antarctic shelf ice, J. Geophys. Res., 107, 1–13, doi:10.1029/2000JB000058, 2002.

Schoof, C.: Ice sheet grounding line dynamics: Steady states, stability, and hysteresis, J. Geophys. Res., 112, 1–19, doi:10.1029/2006JF000664, 2007.

Seroussi, H., Morlighem, M., Rignot, E., Larour, E., Aubry, D., Ben Dhia, H., and Kristensen, S. S.: Ice flux divergence anomalies on 79north Glacier, Greenland, Geophys. Res. Lett., 38, 1–5, 2011.

Seroussi, H., Morlighem, M., Rignot, E., Khazendar, A., Larour, E., and Mouginot, J.: Dependence of century-scale projections of the Greenland ice sheet on its thermal regime, J. Glaciol., 59, 1024–1034, doi:10.3189/2013JoG13J054, 2013.

Seroussi, H., Morlighem, M., Larour, E., Rignot, E., and Khazendar, A.: Hydrostatic grounding line parameterization in ice sheet models, The Cryosphere, 8, 2075–2087, 2014.

Shepherd, A., Wingham, D., and Mansley, J.: Inland thinning of the Amundsen Sea sector, West Antarctica, Geophysical Research Letters, 29, 7–10, 2002.

Shepherd, A., Ivins, E. R., A, G., Barletta, V. R., Bentley, M. J., Bettadpur, S., Briggs, K. H., Bromwich, D. H., Forsberg, R., Galin, N., Horwath, M., Jacobs, S., Joughin, I., King, M. a., Lenaerts, J. T. M., Li, J., Ligtenberg, S. R. M., Luckman, A., Luthcke, S. B., McMillan, M., Meister, R., Milne, G., Mouginot, J., Muir, A., Nicolas, J. P., Paden, J., Payne, A. J., Pritchard, H., Rignot, E., Rott, H., Sø rensen, L. S., Scambos, T. a., Scheuchl, B., Schrama, E. J. O., Smith, B., Sundal, A. V., van Angelen, J. H., van de Berg, W. J., van den Broeke, M. R., Vaughan, D. G., Velicogna, I., Wahr, J., Whitehouse, P. L., Wingham, D. J., Yi, D., Young, D., and Zwally, H. J.: A reconciled estimate of ice-sheet mass balance., Science (New York, N.Y.), 338, 1183–9, 2012.

Tinto, K. J. and Bell, R. E.: Progressive unpinning of Thwaites Glacier from newly identified offshore ridge: Constraints from aerogravity, Geophys. Res. Lett., 38, 1–5, doi:10.1029/2011GL049026, 2011.

van der Veen, C. J.: Fracture mechanics approach to penetration of bottom crevasses on glaciers, Cold Reg. Sci. Technol., 27, 213–223, 1998a.

van der Veen, C. J.: Fracture mechanics approach to penetration of surface crevasses on glaciers, Cold Reg. Sci. Technol., 27, 31–47, 1998b.

van der Veen, C. J. and Whillans, I. M.: Force budget: I. Theory and numerical methods, J. Glaciol., 35, 53–60, 1989.

Vaughan, D. G., Corr, H. F. J., Bindschadler, R. A., Dutrieux, P., Gudmundsson, G. H., Jenkins, A., Newman, T., Vornberger, P., and Wingham, D. J.: Subglacial melt channels and fracture in the floating part of Pine Island Glacier, Antarctica, J. Geophys. Res. - Earth Surface, 117, doi:10.1029/2012JF002360, 2012.

Vogel, C. R.: Computational Methods for Inverse Problems, Society for Industrial and Applied Mathematics, Philadelphia, PA, USA, 2002.

Weertman, J.: On the sliding of glaciers, J. Glaciol., 3, 33–38, 1957.

Weertman, J.: Can a water-filled crevasse reach the bottom surface of a glacier?, IASH Publ, 95, 139–145, 1973.

Weertman, J.: Stability of the junction of an ice sheet and an ice shelf, J. Glaciol., 13(67), 3–11, 1974.

Weiss, J.: Subcritical crack propagation as a mechanism of crevasse formation and iceberg calving, 50, 109–115, 2004.

~~Experiment characteristics Experiment Set Number of Experiments Experiment Characteristics A 11 Current geometry with micro initial crevassesB 7 4 km ice shelfC 4 2 km ice shelfD 7 3 m initial surface crevasseE 7 4 km ice shelf with 400 m high, 400 m wide undercutting~~

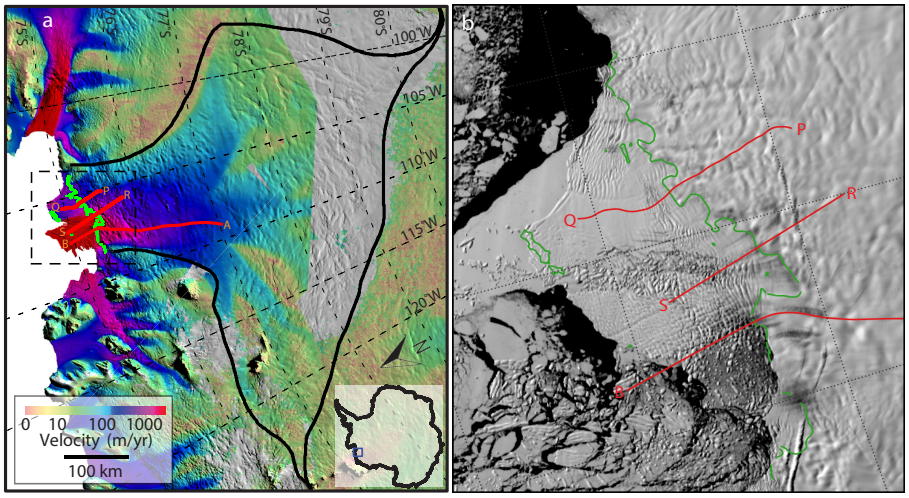

Figure 1. Velocity map and MODIS image of Thwaites Glacier (TG), West Antarctica. a) Velocity field of TG derived from InSAR with data collected in 2008 (Rignot et al., 2011b). The black contour is the drainage basin of TG. b) MODIS image of the dashed box region in a) on Nov. 01, 2012. PQ and RS are the flight tracks of the echograms shown in Fig. 2. AB is the selected flowline of this study. The green line is the grounding line of TG in 2011 (Rignot et al., 2011a).

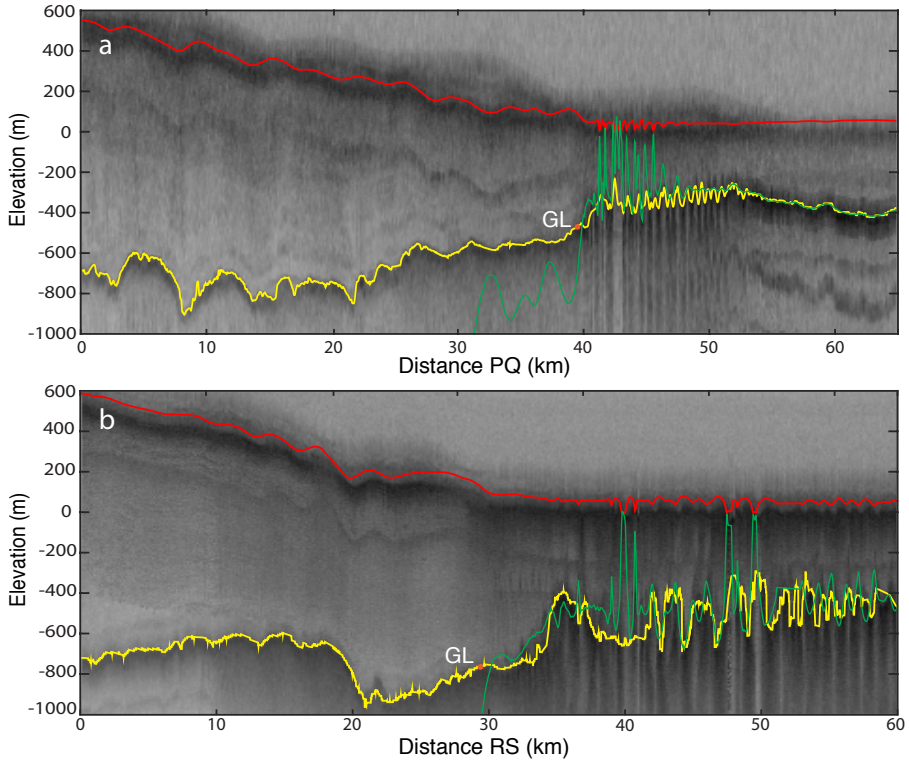

Figure 2. Two echograms of Thwaites Glacier (TG). a) Echogram of flight track PQ on Nov.02, 2009. b) Echogram of flight track RS on Nov.19, 2010. The red lines are ice surface elevation measured by Airborne Topographic Mapper (ATM) (Krabill, 2014) and the green lines are bed elevation calculated from hydrostatic equilibrium. The ~~blue~~ yellow lines are the elevation of ice bottom measured by ice radar depth sounder (Gogineni, 2012). The ~~green~~ orange dots are the grounding line positions in 2011 (Rignot et al., 2011a).

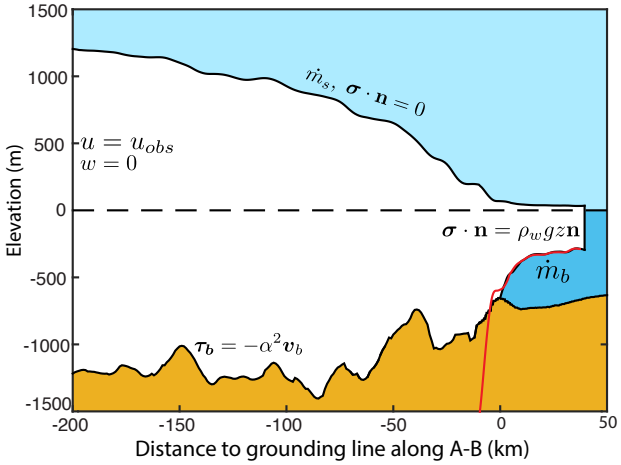

Figure 3. Geometry of the selected flowline AB and boundary conditions of the model. The black lines are ice surface elevation, ice bottom elevation and bed elevation. The red line is the hydrostatic ~~bed~~ bottom elevation calculated from surface elevation.

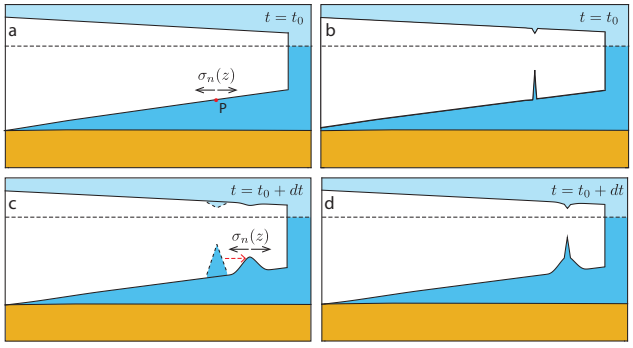

Figure 4. Schematic of the combination of ISSM and LEFM. a) Initial condition, b) Crevasses propagate, c) Crevasses advect downstream, d) Crevasses grow.

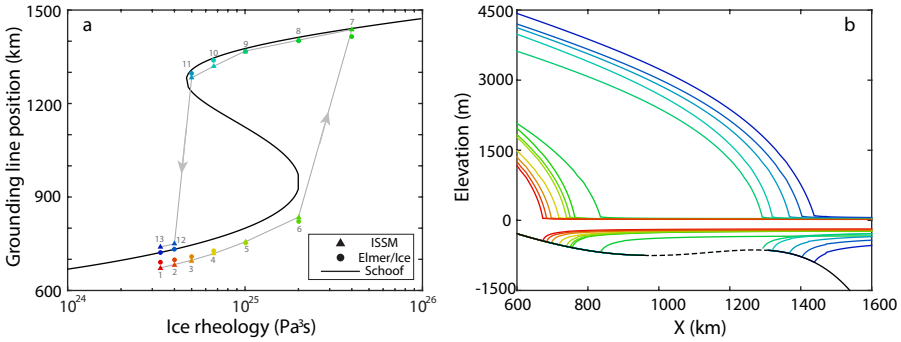

Figure 5. Results of MISMIP Exp 3. a) Steady state grounding line positions of MISMIP Exp ~~3 obtained by~~ 3. Triangles are results of ISSM~~(blue dots) compared with~~ ; circles are results of the FS solution of Elmer/Ice Durand et al. (2009a) ~~(red dots)~~ and ~~Schoof (2007) solution (~~the black curve ~~)~~ is Schoof (2007) solution (Pattyn et al., 2012). The gray arrow shows the sequence of ice rheology perturbation at each step. b) Steady state profile at each step obtained by ISSM. The retrograde part of the bed is shown in dashed line.

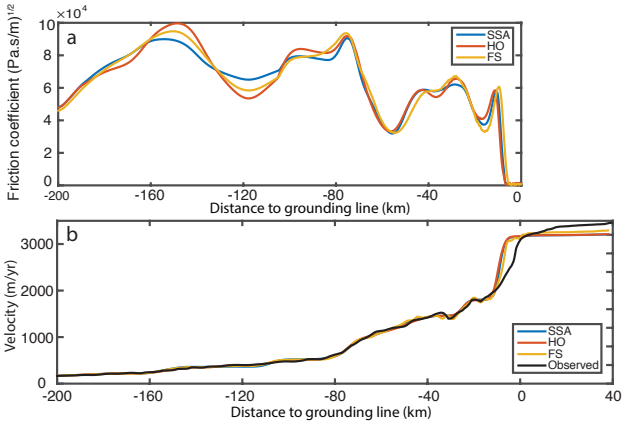

Figure 6. Inversion results of basal friction on flowline AB. a) Friction coefficient inferred with all three models (FS, HO and SSA). b) Comparison of modeled surface velocity and observed surface velocity for all three models.

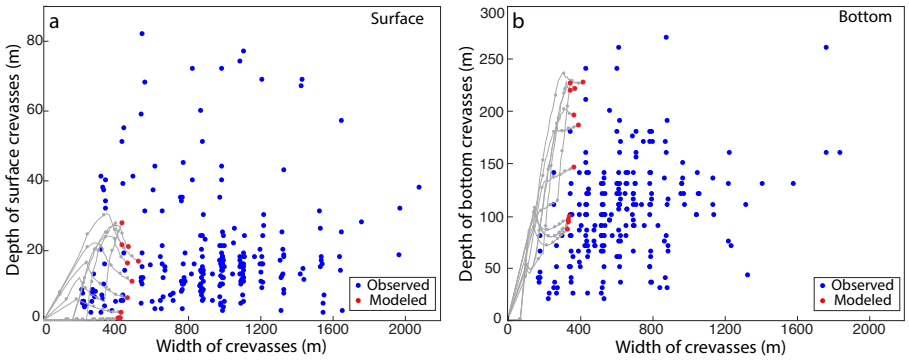

Figure 7. Comparison of the shape of observed and modeled crevasses. a) Depth and width of surface crevasses. b) Depth and width of bottom crevasse. Blue dots are observed crevasses and red dots are modeled crevasses. Gray lines and gray dots are the evolution of the shape of modeled crevasses.

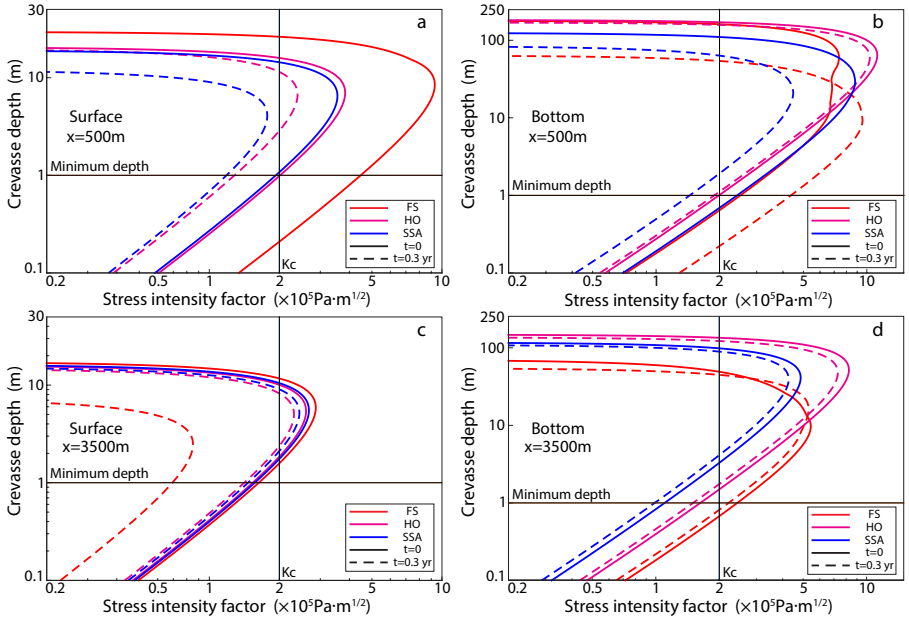

Figure 8. Stress intensity factor as a function of depth. a) Surface crevasse with initial crevasse position at x=500 m. b) Bottom crevasse with initial crevasse position at x=500 m. c) Surface crevasse with initial crevasse position at x=3500 m. d) Bottom crevasse with initial crevasse position at x=3500 m. Red, blue and magenta lines are corresponding to the FS, HO and SSA model. Solid and dashed lines are corresponding to the beginning and the end of each simulation. The crevasse propagates if its minimum required depth is smaller than 1 m. (The stress intensity factor for surface crevasse of FS at x=500 m, t=0.3 yr is not shown because it is negative at all depth.)

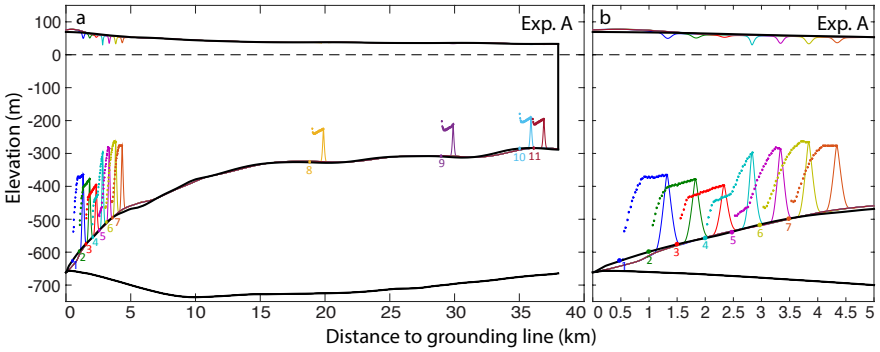

Figure 9. Crevasse propagation with the initial geometry of flowline AB. a) Crevasse propagation of Exp. A1–A11 with FS. Each color corresponds to one initial crevasse position, indicated by the number. The solid lines are the shape of final crevasses. The dotted lines are the evolution of the tips of bottom crevasses. b) Details of the grounding line region for Exp. A1-A7. The black lines are the initial geometry for ice surface, ice bottom and seafloor.

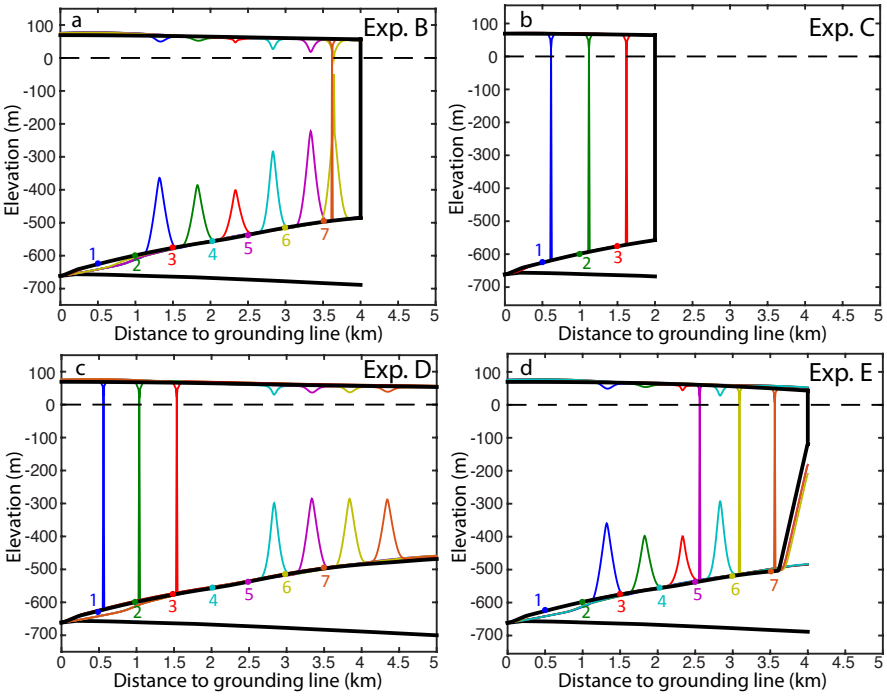

Figure 10. Crevasse propagation in the grounding line region with varying initial geometry. In each panel, solid lines are the shape of final crevasses with a) 4 km long ice shelf (Exp. B1–B7), b) 2 km long ice shelf (Exp. C1–C3), c) 3 m deep, 100 m wide initial surface crevasse (Exp. D1–D7), and d) 4 km long ice shelf with a 400 m wide and 400 m high undercut ice front (Exp. E1–E7). The black lines are the initial geometry for ice surface, ice bottom and seafloor.